Geochemistry, Geophysics, Geosystems®

Key Points:

- Geochemical and isotopic monitoring of Peteroa volcano allowed us to elaborate a conceptual model that explains the evolution of the magmatic-hydrothermal system
- Fumarolic gases exhibit different compositions during quiescent and unrest/eruptive periods, allowing the identification of precursory signals of the last eruption
- Despite variations in activity, the deep magmatic gas source of Peteroa volcano remained relatively constant, as indicated by consistent He and C isotopic values

Correspondence to:
M. Agusto,
magusto@gl.fcen.uba.ar

Eleven-Year Survey of the Magmatic-Hydrothermal Fluids From Peteroa Volcano: Identifying Precursory Signals of the 2018–2019 Eruption

Mariano Agusto[1,2] , **María Clara Lamberti**[1,2] , **Franco Tassi**[3,4], **Fabricio Carbajal**[5], **Joaquín Llano**[1,2], **Victoria Nogués**[2], **Nicolás Núñez**[6], **Hernán Sánchez**[6], **Andrea Rizzo**[7], **Sebastián García**[5] , **Jazmín Yiries**[1,2], **María Laura Vélez**[1], **Antonella Massenzio**[1,2], **Gabriela Velasquez**[8], **Claudia Bucarey**[8], **Martín Gómez**[6], **Pablo Euillades**[9], and **Víctor Ramos**[1,2]

[1]Departamento de Ciencias Geológicas, Facultad de Ciencias Exactas y Naturales, Universidad de Buenos Aires, Buenos Aires, Argentina, [2]Instituto de Estudios Andinos "Don Pablo Groeber" (IDEAN), CONICET—Universidad de Buenos Aires, Buenos Aires, Argentina, [3]Università degli Studi di Firenze, Firenze, Italia, [4]CNR-IGG Institute of Geosciences and Earth Resources, Florence, Italy, [5]SEGEMAR, Observatorio Argentino de Vigilancia Volcánica (OAVV), Buenos Aires, Argentina, [6]Comisión Nacional de Energía Atómica (CNEA), ICES, Buenos Aires, Argentina, [7]Department of Earth and Environmental Sciences, University of Milano-Bicocca, Milan, Italy, [8]SERNAGEOMIN, Observatorio Volcánico de los Andes del Sur (OVDAS), Temuco, Chile, [9]Facultad de Ingeniería, Instituto CEDIAC, Universidad Nacional de Cuyo, Mendoza, Argentina

Abstract Over the past decade, we have conducted geochemical and isotopic monitoring of the fumarolic gases of the Peteroa volcano (Argentina-Chile). Using the resulting data set, we constructed a conceptual model that describes the evolution of the magmatic-hydrothermal system and identifies precursory geochemical signals of the last eruption. Our data set includes new chemical and isotopic analyses of fumarolic gas samples collected from 2016 to 2021, as well as previously published data from the 2010–2015 period. After an eruptive period in 2010–2011, the activity was characterized by low degassing rates and seismic activity. However, an increase in seismic activity and fumarolic gas emissions was observed from 2016 to 2018–2019 eruptive episode, leading to a major phreato-magmatic eruption. Fumarole gases show different compositions during quiescent versus unrest/eruptive degassing related to the interaction of deep (magmatic) and shallow (hydrothermal) fluid contributions. During quiescent periods, fumaroles exhibited low SO_2/H_2S, HF/CO_2, and HCl/CO_2 ratios (<0.1), revealing a dominant hydrothermal contribution. In contrast, during pre-and syn-eruptive periods, fumaroles showed ratios up to 100 times higher indicative of an enhanced magmatic input. When compared to the evolution of the seismic activity, the increment of magmatic-related strong acidic gases suggests repeated inputs of hot magmatic fluids, which are only partially dissolved into the hydrothermal system feeding the fumaroles. Interestingly, the $^3He/^4He$ and $\delta^{13}C$-CO_2 values remained relatively constant during the magmatic and hydrothermal degassing in 2016–2021, suggesting that the deep magmatic gas source did not significantly change throughout variations in Peteroa's activity.

Plain Language Summary The Peteroa volcano is an active volcano located in the southern Andes Mountains of South America. It has erupted multiple times in recent years, but there is limited knowledge about its behavior and potential damage it could cause. To address this, we have been studying the volcano for the past decade using special techniques to examine the gases that come out of the openings in the ground, known as fumaroles. These fumaroles allow volcanic gases to escape, and by collecting data on fumarolic gas samples from 2010 to 2021, we have developed a model that helps us understand how the volcano changes over time and identify warning signs of an upcoming eruption. Our research found increased seismic activity and fumarolic gas emissions starting in 2016, leading to a significant eruption from 2018 to 2019. We also discovered that the composition of the fumarolic gases varies depending on whether the volcano is in a quiet or unrest period. During quiet periods, the gases show compositions with a stronger influence from underground water, but before and during the 2018–2019 eruption, the gas compositions showed changes indicating a more significant influence of magma. This study is vital as it enhances our understanding of volcano behavior and provides valuable insights for forecasting future eruptions. This is particularly important in the region as there are many potentially dangerous volcanoes with limited available information, but the findings can be applied to improve our understanding of other volcanoes, ultimately contributing to the global knowledge base on volcanic processes.

1. Introduction

Early warning signals of changes in the volcano activity are crucial for activating civil protection protocols to mitigate volcanic hazards (McNutt, 2000; Scarpa & Tilling, 1996; Tilling, 2003). Volcanic unrest can manifest on the surface as seismic signals, ground deformation, and changes in the composition of gases and their emission rates. The chemical and isotopic composition of fumarolic emissions has been widely demonstrated to provide essential information on the evolution of volcanic plumbing systems, which are often modified by secondary processes, mostly occurring in shallow hydrothermal reservoirs that typically overlie the magmatic systems (Aiuppa et al., 2007; Chiodini et al., 2017; Fischer et al., 2015; Menyailov et al., 1986; Moretti et al., 2013; Ohba et al., 2019; Rizzo et al., 2015; Todesco, 2009; Vaselli et al., 2010; Villemant et al., 2014; Zelenski & Taran, 2011).

One of the challenges in predicting volcanic eruptions involving magmatic and hydrothermal interactions is the variety of possible processes at play, including hydrothermal sealing (e.g., Turrialba, 2014 eruption; Mick et al., 2021), magmatic gas input into the hydrothermal system (e.g., White Island 2012 eruption; Christenson et al., 2017; Pico do Fogo 2014 eruption; Melián et al., 2021), and magma intrusion (e.g., Ontake volcano 2007 eruption; Nakamichi et al., 2009; Taal volcano eruption 2020; Hernández et al., 2021). A correct interpretation of the complex interaction between ascending magmatic fluids and the shallow liquid-dominated environment requires long-lasting geochemical monitoring that can be challenging in active volcanoes. However, there are limited geological records of long-term gas compositional variations during the transition from quiescence to unrest to eruption.

Peteroa is one of the most active volcanoes in the Argentine-Chilean Andean range and has been the subject of geochemical investigations for 11 years, from 2010 to 2021 (Agusto et al., 2021; Haller & Risso, 2011). This period includes a phreatic event in 2010–2011 and a phreato-magmatic event in 2018–2019 (Romero et al., 2020). Such an extended geochemical data set, consisting of chemical and isotopic analyses of fluids from vents occurring in the summit craters of the volcano, was compiled as part of various investigation programs involving the Argentine-Italian research group authoring this paper. The main aims of this study are (a) to elaborate a conceptual model that explains the evolution of the magmatic-hydrothermal system in 2016–2021, including the mechanisms that triggered the eruptive phase in 2018–2019 and (b) to obtain information about precursory signals for eruptive phases to be used for geochemical monitoring purposes.

2. Geological Setting and Current Degassing Activity

Peteroa volcano is part of the Planchón—Peteroa Volcanic Complex (PPVC), which is located in the northern segment of the Southern Volcanic Zone (SVZ) of the Andes, including the Azufre, Planchón and Peteroa volcanoes (Figure 1). The PPVC has a range of ages spanning from the Middle Pleistocene to the present, and Peteroa is the youngest volcano (Hildreth et al., 1984; Klug et al., 2018; Naranjo et al., 1999). This volcano is composed of lavas and pyroclastic units of andesitic-basaltic to dacitic composition. The eruptions during this period originated from the summit crater zone, which comprises four primary craters, specifically Crater 1, 2, 3, and 4, along with a scoria cone (Figure 1; Naranjo et al., 1999). Peteroa generated less than 1 km^3 of lavas of mostly andesitic composition (Naranjo et al., 1999). It also generated the most differentiated units within the pyroclastic rocks of the PPVC: Holocene tuffs and unconsolidated deposits of rhyodacite composition (Haller & Risso, 2011; Tormey et al., 1995).

The summit of Peteroa volcano is characterized by acid sulfate thermal lakes (up to 40°C, pH 1–3) and fumarolic fields that emit magmatic-hydrothermal fluids, including an area between Craters 2 and 4 that has been active since at least 2010 (see Figure 1). Previous studies (Aguilera et al., 2016; Benavente, 2010; Tassi et al., 2016) have shown that gases from fumarolic vents have outlet temperatures up to 90°C and are dominated by water vapor (up to 85%) with significant concentrations of acid gases (CO_2, SO_2, H_2S, HCl, and HF). In addition, a profuse diffuse soil gas emission of over 6 tonnes/day of CO_2 has been reported between Craters 2 and 4 (Lamberti et al., 2021). Recent observations (Agusto et al., 2021) have also documented a new (ephemeral) fumarolic field between Craters 1 and 3 with gas compositions similar to those previously described.

Two thermal areas are also recognized at the foothills of the eastern flank of PPVC, which host thermal waters (up to 50°C; pH 5–7), bubbling gases with a CO_2-dominated composition (Benavente, 2010; Llano et al., 2021; Nogués, 2019) and soil diffuse CO_2 anomalies (Lamberti et al., 2021) with a structural control (Vigide et al., 2020).
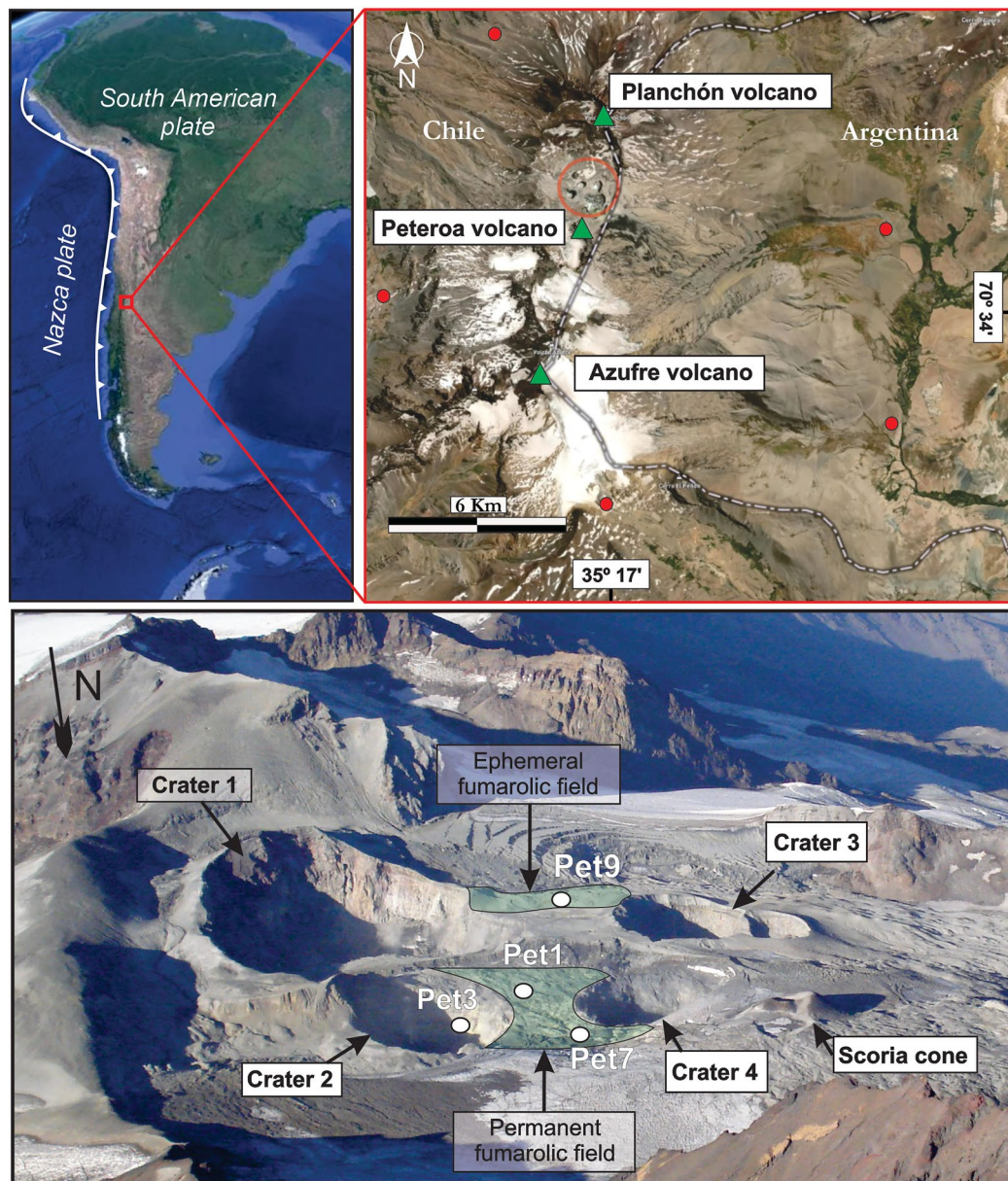
Figure 1. Location of Azufre, Peteroa, and Planchon volcanoes at PPVC. The red circle in the upper right satellite overview points out the crater zone of Peteroa volcano. Red dots in the satellite overview point out volcanic monitoring stations (IP camera, seismometers and GNSS) from SERNAGEOMIN-OVDAS and SEGEMAR-OAVV. Below: Aerial view of the crater zone of Peteroa volcano. Craters 1, 2, 3, and 4, the scoria cone and the location of two fumarolic fields and main fumaroles (Pet1, 3, 7, and 9 in white dots) are indicated in the photograph.

3. Eruptive Events Prior to 2018

Peteroa volcano has experienced at least 18 phreatic and phreatomagmatic eruptions in historical times, from 1660 to 1998 (González-Ferrán, 1995; Naranjo & Haller, 2002; Naranjo et al., 1999). The average repose time for the past 420 years is 18 years, but it decreased to around 9 years between 1937 and 2010 (Haller & Risso, 2011). The most critical seismic event affecting the study area ever recorded occurred in February 2010 (Maule earthquake, 8.8 Mw). This devastating earthquake likely triggered the 2010–2011 (VEI 1–2) Peteroa eruptive events (Aguilera et al., 2016; Tassi et al., 2016) as well as other eruptions in the region (e.g., Cordón Caulle volcano 2011, Bonali et al., 2013; Copahue volcano 2012, Agusto et al., 2017; Caselli et al., 2016).
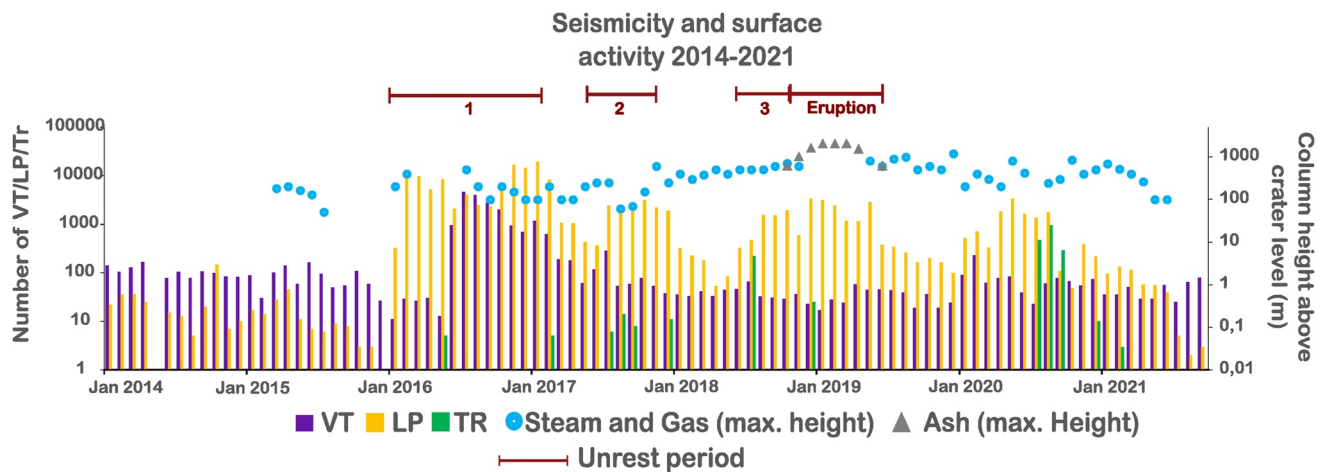
Figure 2. Temporal evolution of seismic events and crater fluid emissions between January 2014 and April 2021. The total number of seismic events (LP long period, TR tremor, and VT volcano tectonic) is reported per month. The column height corresponds to the highest value recorded per month. The three main unrest periods (January 2016–February 2017; June 2017–December 2017; May 2018–November 2018) and the December 2018–May 2019 eruption are indicated. Data from SERNAGEOMIN-OVDAS and SEGEMAR-OAVV reports, see details in text.

During the 2010–2011 eruption, a few seismic swarms were recorded in the PPVC area concentrated in two main zones, located 16–33 km NE and 5–7 km N of the crater area, with foci situated at depths of 1–30 km and 1–8 km, respectively. Most of these earthquakes (nearly 85%) were interpreted as produced by rock fracturing, while a few were related to underground fluid circulation (SERNAGEOMIN-OVDAS reports, 2010-2011; Tassi et al., 2016). However, it is worth noting that the seismological information came from regional seismic stations located outside the study area since continuous seismological monitoring of the Peteroa volcano began in 2014 (SERNAGEOMIN-OVDAS reports).

The 2010–2011 eruptive period was characterized by four explosive eruptive phases dominated by low-intensity phreatic activity, which produced almost permanent gas/steam columns that rose from 200 to 800 m above the active crater. Those columns frequently contained low ash amounts and were occasionally interrupted by phreatic explosions that produced ash columns up to 3,000 m high during the more intense periods. The eruptive plumes were mainly transported to NE, E, and SE, according to the regional wind regime, and were observed as far as 638 km from the active crater (Aguilera et al., 2016). In the post-eruptive period (2012–2013), the gases from the Peteroa summit showed a considerable increase in the acidic gases, apparently indicating a late magmatic fluids pulse (Tassi et al., 2016).

4. The 2018–2019 Eruption

After a continuous quiescent 2013–2016 period, three periods of unrest were recognized at the Peteroa volcano between 2016 and 2019 based on seismic activity (Figure 2), with the final unrest period immediately followed by the 2018–2019 eruptive episode (Forte et al., 2022; Romero et al., 2020; SEGEMAR-OAVV reports, 2019-2021; SERNAGEOMIN-OVDAS reports, 2010-2021). During these periods, no significant deformation was detected at the SERNAGEOMIN-OVDAS GNSS stations located near the volcano. We confirmed this observation by independently processing Sentinel 1 scenes acquired between 2014 and 2020.

The first unrest period started in January 2016 with an increase in earthquakes related to fluid dynamics inside the volcano, consisting of long period (LP), very long period (VLP) and tremor (TR) activity (SERNAGEOMIN-OVDAS reports, 2016). During June 2016, volcano tectonic (VT) signals increased, indicating brittle rock fracture within the volcanic complex. Sporadic gas and water vapor emissions reaching heights of up to 500 m above the crater were observed by IP cameras from a multiparametric scientific station from CNEA-ICES (Argentina).

In June 2017, a second unrest period started with an increase in LP and VT signals, which lasted until December 2017. Then, VT number events strongly decreased, while LP events remained frequent, showing a peak of activity in October 2017. TR events were also recorded.

In November 2017, emissions of gases and steam columns up to 600 m high occurred. Sentinel 2 L2A images allowed identifying that the sources of these emissions were Craters 1 and 3 (SEGEMAR-OAVV reports, 2019).

During this period, a fumarolic field was established within Crater 1, similar to the pre-existing fumarolic field in Crater 3. Between June and December 2017, a rapid increase in heat flux values, from 0.34 to 20 MW, was observed in Crater 3 by processing satellite images (Landsat and Planet Labs Inc. imagery; Aguilera et al., 2021).

The third unrest period started in mid-May 2018 and was characterized by continuous TR close to the crater area. On 21 June 2018, a TR-type event was observed, characterized by a 500-m-high gas/steam emission column. This event is possibly related to a phreatic explosion and likely played a role in the subsequent development of a nested crater on the southern wall of Crater 1 (Figure 3). The LP seismicity showed a marked increase in the number of events from August 2018, reaching two maximum peaks in September and December 2018. The latter was preceded by phreatomagmatic explosion occurred on 7 November 2018.

Throughout 2018, both Crater 3 and the fumarole field situated between Craters 2 and 4 were affected by intense degassing, as reported by Bobrowski et al. (2019) and Agusto et al. (2021). Furthermore, these authors identified the emergence of a new, ephemeral fumarolic field between the southern flanks of Craters 1 and 3 (Figure 1). Satellite images support these observations of enhanced activity showing the occurrence of thermal anomalies in Crater 3 and Crater 1 in July and December 2018, respectively (Aguilera et al., 2021).

On 14 December 2018, Peteroa volcano exhibited incandescence and a pulsating column from Crater 1 consisting mainly of ash (CNEA-ICES IP cameras, and SEGERMAR-OAVV reports, 2018). This event was accompanied by an increment of LP number events followed by spasmodic TR-type events (Figure 2), with a shallow source close to the crater zone. By the end of December 2018, proximal ash fall deposits comprised 10% juvenile material, decreasing to 6% in January as the eruption progressed (Romero et al., 2020). In February 2019, the eruption activity peaked, with continuous ash emission forming a column that reached a height of 2,000 m, accompanied by intense LP events.

In March 2019, the emitted particulate material changed from gray to reddish in color (Figure 3), which was characterized by 5% of juvenile material. According to Romero et al. (2020), the 2018/2019 juvenile fragments correspond to andesite to basaltic-trachyandesite composition from the high-K calc-alkaline series. Properties of the juvenile material indicated phreatomagmatic eruption processes, in contrast to the 2010–2011 phreatic activity (Romero et al., 2020). The activity was constant until April 2019, when steam and ash emissions became sporadic, and the LP and TR seismic activity decreased. Finally, minor explosions with ash emissions were recorded at least until mid-May 2019 (Forte et al., 2022).

From then until 2022, the behavior of the Peteroa volcano was characterized by sporadic gaseous emissions that reached a height of up to 800 m above the crater. Additionally, degassing from the ephemeral fumarolic field between Craters 1 and 3 has become intermittent, with only a few isolated gas emissions observed.

5. Materials and Methods

5.1. Gas Sampling

From March 2016 to April 2021 seven gas samples were collected from two fumaroles, one (Pet1) pertaining to the permanent fumarolic field located between Crater 2 and Crater 4, the second (Pet9) from the area between Crater 1 and Crater 3 characterized by the ephemeral emission (Figure 1). The sampling and analytical procedures adopted for the gases constituting the new data set (from 2016 to 2021) were similar to those used to produce the 2010 to 2015 data set previously published by Tassi et al. (2016). The gas sampling line consisted of a 0.6 m long titanium tube ($\emptyset$ = 2.5 cm) and pyrex glass dewared pipes connected to pre-weighed and pre-evacuated 60-mL glass Thorion®-tapped flasks filled with 20 mL of 4 N NaOH and 0.15M Cd(OH)$_2$ suspension (Montegrossi et al., 2001; Vaselli et al., 2006). This technique allows to separate SO$_2$ and H$_2$S in situ, the latter forming insoluble CdS, whereas SO$_2$ is dissolved in the NaOH solution with water vapor and other acidic gases (CO$_2$, HCl, HF). The flask head-space contained the low-solubility gas species that do not react with the soda suspension (N$_2$, O$_2$, CO, H$_2$, He, Ar, CH$_4$ and light hydrocarbons). A water-cooled condenser connected to the sampling line allowed the collection of an aliquot of condensate (for the analysis of F$^-$, Cl$^-$, δ^{18}O-H$_2$O and δD-H$_2$O) and dry gas (after removal of condensable species, for analysis of δ^{13}C–CO$_2$ and He isotopes).
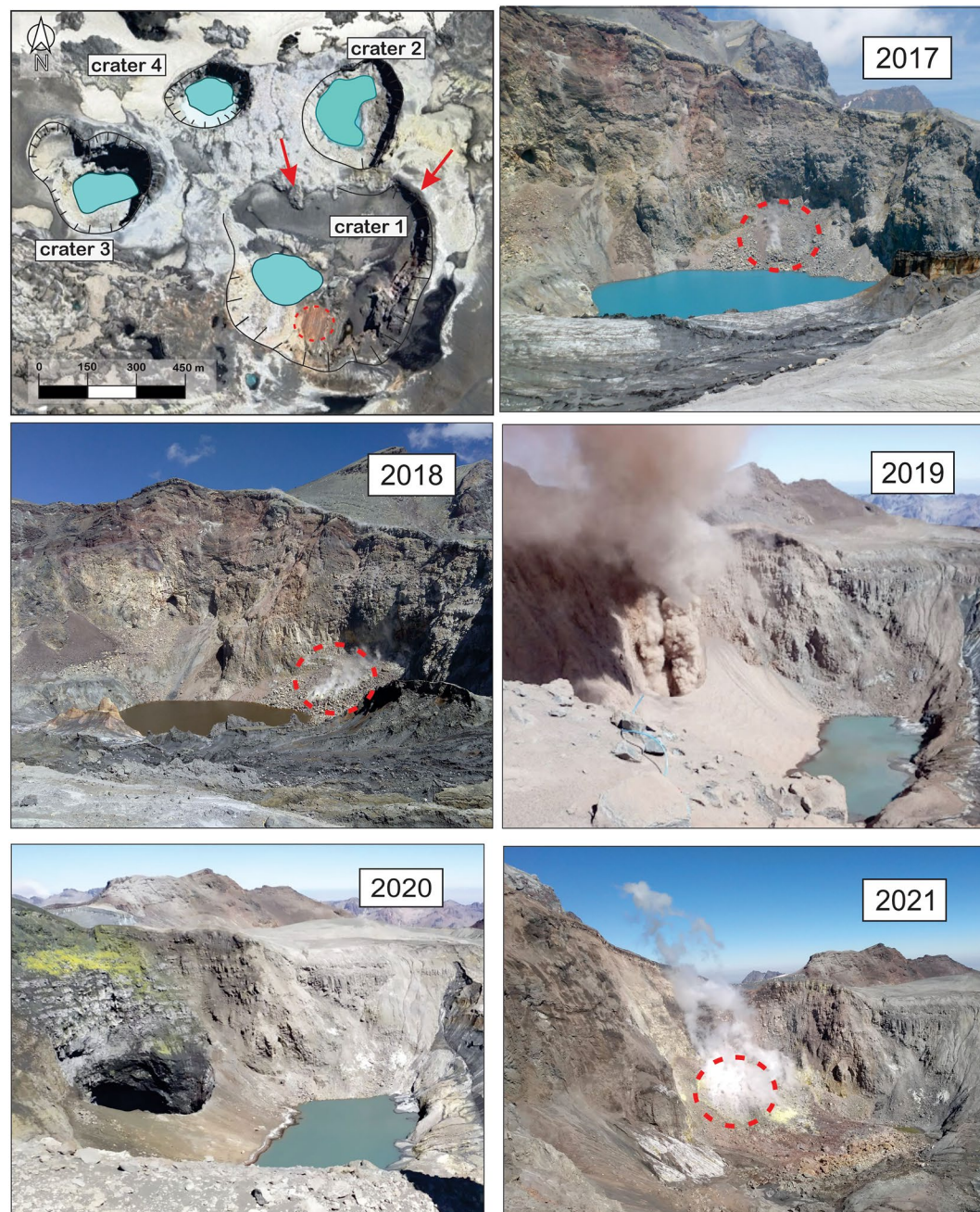
Figure 3. On the upper left, the satellite overview displays a detail of the craters of the Peteroa volcano, where the red arrows indicate the lines of sight SW (2017–2018) and SE (2019–2021) perspectives of photographs taken of the Crater 1. Additionally, the red dashed circle highlights the area of fumaroles inside Crater 1 at the vent site of the 2018–2019 eruption. Note the reddish ash-rich eruption column in 2019 and the post-eruption open vent in 2020.

5.2. Analytical Methods

Inorganic (N_2, Ar, O_2, H_2, He, and CO) and organic (C_1-C_3 hydrocarbons) gases from the flask headspace were analyzed at the Fluid Geochemistry Laboratory of the University of Florence (Italy) using gas chromatography (GC: Shimadzu 15A, Shimadzu 14, and Thermo Focus). The liquid and the solid phases of the suspension were separated by centrifugation, to analyze CO_2, SO_2, HCl, and HF, as CO_3^{2-} (by acidimetric titration, AT; Metrohm Basic Titrino), SO_4^{2-}, Cl^- and F^- (by ion chromatography, IC; Metrohm 761), respectively. The CdS precipitate was dissolved by oxidation with H_2O_2 to analyze H_2S as SO_4^{2-} by IC. The analytical error for GC, AT, and IC

analyses was <5% (Tassi et al., 2016). In the condensates, the analysis of F⁻ for the determination of HF was carried out by IC, whereas the $\delta^{18}O$ and δD values in water vapor ($\delta^{18}O$-H_2O and δD-H_2O, expressed as ‰ vs. V-SMOW) were determined using a Finnigan Delta Plus XL mass spectrometer at the Geokarst Engineering Laboratory (Trieste, Italy) following the methods described by Epstein and Mayeda (1953) and Coleman et al. (1982), respectively.

The $\delta^{13}C$–CO_2 values in the dry gases were determined at the Laboratory of Stable Isotopes of CNR-IGG in Pisa (Italy) by using a Finnigan Delta S mass spectrometer (MS), after extracting and purifying CO_2 by using liquid N_2 and N_2- trichloroethylene cryogenic traps (Evans et al., 1998; Vaselli et al., 2006). Carrara and San Vincenzo marbles, as well as international NBS18 and NBS19 standards, were used to estimate the external precision. Analytical uncertainty and the reproducibility were ±0.05‰ and ±0.1‰, respectively.

The $^3He/^4He$ (expressed as R/Ra, where R is the $^3He/^4He$ measured in the sample and Ra is the $^3He/^4He$ ratio in the air: 1.39×10^{-6}; Mamyrin & Tolstikhin, 1984) and $^4He/^{20}Ne$ ratios were determined at the Laboratory of Noble gas isotopes of INGV in Palermo (Italy), by separately introducing He and Ne into a split-flight-tube mass spectrometer (GVI Helix SFT) after performing standard purification procedures (Rizzo et al., 2015). The analytical error on $^3He/^4He$ was ≤1%, while on ^{20}Ne was <0.1%. The measured R/Ra values were corrected for air contamination using the $^4He/^{20}Ne$ ratios (Poreda & Craig, 1989), as follows:

$$Rc/Ra = [(R/Ra) - r)]/(1 - r) \tag{1}$$

where $r = (^4He/^{20}Ne)_{air}/(^4He/^{20}Ne)_{meas}$, the $(^4He/^{20}Ne)_{air}$ ratio being that in the atmosphere (0.318; Ozima & Podosek, 1983) and the $(^4He/^{20}Ne)_{meas}$ ratio that measured in the gas sample. Argon isotopes (^{40}Ar, ^{38}Ar, ^{36}Ar) were measured in a Helix MC-GVI mass spectrometer, with an analytical uncertainty <0.2% (Rizzo et al., 2019).

6. Results

Table 1 presents an overview of the outlet temperatures, chemical composition of the dry fraction, and steam concentrations (expressed in mmol/mol) of gases collected for Pet1 (from March 2016 to April 2021) and Pet9 fumaroles (2018). Additionally, the analytical data of fumarolic gases collected in February 2010–April 2015 (Tassi et al., 2016) are also reported.

The outlet temperatures of the Peteroa crater fumaroles ranged from 78 to 90°C, the highest corresponding to the boiling temperature of pure water at altitudes of 3,500 m. The chemical composition was dominated by water vapor with a gas fraction up to 15%. Dry gases mainly consisted of CO_2 (up to 980 mmol/mol) and significant concentrations of H_2S (11–162 mmol/mol), SO_2 (0.1–534 mmol/mol), HCl (0.1 and 14 mmol/mol) and HF (0.01 and 1.3 mmol/mol). The concentrations of N_2, CH_4, and H_2 were relatively constant ranging from 1.6 to 9.5, from 0.12 to 1.8, and from 0.13 to 0.47 mmol/mol, respectively. Minor amounts of Ar, He, and CO were also present, with concentrations up to 0.0064, 0.0041, and 0.015 mmol/mol, respectively.

Table 2 lists the isotopic compositions of noble gases (He, Ar, Ne) and $\delta^{13}C$–CO_2 for gas samples collected from March 2016 to April 2021 and those reported by Tassi et al. (2016). The Rc/Ra values range from 4.43 to 7.11, with negligible air contamination, as indicated by the relatively high $^4He/^{20}Ne$ ratios (from 55 to 711). During the period 2015–2021, the Rc/Ra and $\delta^{13}C$–CO_2 values varied in a relatively narrow range between 6.11 and 6.71, and from −7.54 to −6.15‰ versus V-PDB, respectively, which were similar to the values reported for the period 2010–2015, except for samples collected in 2012, which were significantly lower (up to −11.6‰ vs. V-PDB). The $^{40}Ar/^{36}Ar$ ratios varied from 395 to 473, being much lower than the expected values for a MORB-like mantle 44,000 (Moreira et al., 1998) and more typical of subduction-related settings (Rizzo et al., 2022 and references therein). The $\delta^{18}O$-H_2O and δD-H_2O values in 2012–2021 period had broad ranges from −10.5 to −17.2‰ and from −119 to −76‰ versus V-SMOW, respectively, whereas in 2011 (Tassi et al., 2016) they were significantly higher (−3.5 to −4.3‰ and −74 to −73‰, respectively).

7. Discussion

7.1. Characterization of the Deep Magmatic Source

The He isotopic signature of the Peteroa fumaroles ($^3He/^4He$ up to 7.11 Rc/Ra) closely resembles that of mantle-related fluids in the Andean SVZ (Barry et al., 2022; Lages et al., 2021; Tardani et al., 2017), providing strong evidence for a significant contribution from a magmatic source, as already suggested by Tassi et al. (2016)

Table 1
Outlet Temperature (in °C), Chemical Composition of the Dry Gas Fraction (mmol/mol) and Total Gas Concentrations (Xg %) of the Peteroa Volcanic Gases

ID	Date	Latitude	Longitude	Altitude	T°	CO_2	HCl	HF	SO_2	H_2S	N_2	CH_4	Ar	O_2	H_2	He	CO	Xgas %	SO_2/H_2S	$100*HCl/CO_2$	$1,000*HF/CO_2$
Pet1	February-2010	6099208	357027	3436	92	978	0.25	0.01	0.12	19	1.6	0.24	0.026	0.056	0.36	0.0032	0.0026	9.5	0.006	0.025	0.011
Pet2	February-2010	6099171	356908	3434	102	961	0.19	0.02	0.17	35	2.7	0.29	0.024	0.049	0.38	0.0028	0.0031	8.9	0.005	0.020	0.022
Pet1	March-2011	6099208	357027	3436	88	975	0.37	0.01	0.55	21	2.6	0.13	0.0043	0.0065	0.25	0.0014	0.015	14.6	0.026	0.038	0.010
Pet3	March-2011	6099212	357037	3374	88	979	0.38	0.01	0.51	18	2.3	0.10	0.0016	0.0047	0.21	0.0012	0.0092	12.1	0.028	0.039	0.012
Pet4	March-2011	6099169	357042	3401	88	978	0.32	0.01	0.40	18	2.5	0.11	0.0042	0.028	0.18	0.0013	0.0089	14.7	0.022	0.033	0.012
Pet5	March-2011	6099157	357050	3331	43	986	0.24	0.01	0.31	11	2.5	0.12	0.0076	0.028	0.13	0.0015	0.0050	21.8	0.028	0.024	0.008
Pet6	March-2011	6099288	357171	3358	88	978	0.31	0.01	0.41	19	2.4	0.10	0.0047	0.0068	0.23	0.0015	0.015	15.0	0.022	0.032	0.010
Pet7	March-2011	6099257	356939	3411	88	980	0.38	0.01	0.54	16	2.3	0.09	0.0043	0.0010	0.28	0.0022	0.012	15.4	0.033	0.039	0.011
Pet1	March-2012	6099208	357027	3436	88	382	14	1.30	448	145	9.5	0.01	0.025	0.0004	0.32	0.0037	0.0012	3.4	3.089	3.660	3.400
Pet3	March-2012	6099212	357037	3374	89	380	13	1.27	450	148	7.3	0.01	0.0079	0.0009	0.23	0.0034	0.0010	2.8	3.047	3.337	3.344
Pet7	March-2012	6099257	356939	3411	88	370	13	1.24	456	153	6.5	0.01	0.0047	0.0005	0.36	0.0036	0.0009	3.8	2.975	3.520	3.351
Pet8	March-2012	6099317	356996	3446	88	282	12	1.23	534	162	7.8	0.02	0.014	0.0007	0.47	0.0043	0.0008	3.0	3.302	4.286	4.351
Pet1	March-2014	6099208	357027	3436	90	916	0.56	0.04	31	47	5.3	0.09	0.007	0.0011	0.41	0.0033	0.0026	5.8	0.660	0.061	0.038
Pet1	April-2015	6099208	357027	3436	88	958	0.31	0.02	1.20	35	4.9	0.16	0.0045	0.0039	0.32	0.0018	0.0074	11.3	0.034	0.032	0.017
Pet7	April-2015	6099212	357037	3374	89	955	0.22	0.02	1.60	39	4.2	0.11	0.0053	0.0025	0.25	0.0017	0.0066	10.4	0.041	0.023	0.018
Pet 1	March-2016	6099208	357027	3436	90	970	0.15	0.01	0.13	26	3.1	0.15	0.0059	0.0061	0.22	0.0014	0.0013	15.1	0.005	0.015	0.012
Pet1	February-2017	6099208	357027	3436	90	973	0.21	0.02	0.26	22	3.3	0.19	0.051	0.0033	0.26	0.0016	0.0078	4.0	0.012	0.022	0.015
Pet1	February-2018	6099208	357027	3436	90	860	3.2	0.60	36	95	3.6	1.20	0.044	0.009	0.21	0.0033	0.0044	4.2	0.379	0.372	0.698
Pet9	February-2018	6099212	357037	3374	89	897	4.1	0.80	24	68	3.5	1.40	0.049	0.011	0.29	0.0025	0.0039	3.6	0.353	0.457	0.892
Pet1	February-2018	6099208	357027	3436	90	861	3.3	0.50	41	89	3.1	1.30	0.058	0.006	0.23	0.0036	0.0048	2.9	0.461	0.383	0.581
Pet9	February-2018	6099212	357037	3374	89	887	4.2	0.90	29	72	3.9	1.80	0.064	0.014	0.34	0.0021	0.0034	3.0	0.403	0.474	1.015
Pet1	February-2019	6099208	357027	3436	82	867	3.6	0.50	16	105	6.6	1.10	0.045	0.015	0.34	0.0031	0.0031	3.8	0.152	0.415	0.577
Pet1	March-2019	6099208	357027	3436	82	876	3.3	0.70	15	101	2.9	0.36	0.031	0.007	0.31	0.0041	0.0029	3.5	0.149	0.377	0.799
Pet1	April-2021	6099208	357027	3436	78	960	0.21	0.01	0.55	31	5.6	1.20	0.019	0.007	0.25	0.0028	0.0051	4.2	0.018	0.022	0.014

Note. Ratios of main acid gases are also reported. Samples 2010–2015 from Tassi et al. (2016), 2016–2021 this work.

Table 2
Isotopic Composition of Peteroa Fumarole Gas Discharges

ID	Date	R/Ra	Rc/Ra	$^{40}Ar/^{36}Ar$	$^{4}He/^{20}Ne$	$\delta^{13}C$-CO_2	δD-H_2O	$\delta^{18}O$-H_2O	$CO_2/^3He \times 10^{10}$	% He_crust	% He_atm	% He_magma
Pet3	March-2011	6.87	6.87	455	711	−7.60	−73	−4.3	8.5	14.1	<0.1	85.9
Pet5	March-2011	7.10	7.11	378	289	−3.56	−74	−3.5	6.7	11.1	0.1	88.9
Pet7	March-2011	6.59	6.59	491	511	−5.82	n.a	n.a	4.9	17.6	<0.1	82.3
Pet1	March-2012	4.43	4.43	313	305	−11.2	−115	−15.7	1.7	44.6	0.1	55.3
Pet3	March-2012	4.46	4.46	337	387	−11.2	−76	−10.5	1.8	44.3	0.1	55.7
Pet7	March-2012	4.46	4.46	367	662	−11.6	−98	−13.4	1.7	44.3	<0.1	55.7
Pet8	March-2012	4.44	4.44	314	398	−11.4	−103	−15.1	1.4	44.5	<0.1	55.4
Pet7	March-2014	5.62	5.62	n.a	454	n.a	n.a	n.a	3.6	29.8	<0.1	70.2
Pet1	April-2015	6.68	6.68	n.a	456	−7.54	−98	−13.7	5.7	16.5	<0.1	83.5
Pet7	April-2015	6.51	6.51	n.a	511	−6.15	−119	−17.2	6.2	18.6	<0.1	81.3
Pet1	March-2016	6.11	6.11	n.a	356	−6.66	n.a	n.a	8.2	23.6	0.1	76.3
Pet1	February-2017	6.30	6.33	431	155	−6.21	−111	−15.5	6.9	20.4	0.5	79.0
Pet1	February-2018	6.70	6.71	473	131	−6.15	n.a	n.a	2.8	16.0	0.2	83.8
Pet1	February-2019	6.57	6.58	444	155	−7.01	−99	−13.9	3.1	17.6	0.2	82.2
Pet1	March-2019	6.65	6.66	413	256	−6.66	−97	−13.3	2.3	16.7	0.1	83.2
Pet1	April-2021	6.40	6.41	395	290	−6.33	n.a	n.a	3.8	19.8	0.1	80.1

Note. Air-corrected $^3He/^4He$ are reported as Rc/Ra values (Ra being the atmospheric He isotopic ratio). $^{40}Ar/^{36}Ar$, $^{4}He/^{20}Ne$, $\delta^{13}C$-CO_2 expressed as ‰ versus V-PDB, δD-H_2O and $\delta^{18}O$-H_2O expressed as ‰ versus SMOW, and $CO_2/^3He$ ratios are reported. Also shown are the relative contributions of different He sources (%) as calculated in the text, see Section 7.1. n.a: not analyzed.

(Figure 4). The Rc/Ra values of the Peteroa gases are the highest in the northern segment of the SVZ (e.g., Tinguiririca, San José, Campanario, in Benavente et al. (2015)), and in the range of other high values of fumarolic summit compositions of the SVZ such as Copahue, Toluca and Pelehue (Agusto et al., 2013; Roulleau et al., 2016; Tardani et al., 2017; Tassi et al., 2017).

According to the R/Ra signature inferred for the mantle below the Andean region (8 ± 1 Ra; Barry et al., 2022; Lages et al., 2021), the fraction of atmospheric (*a*), magmatic (*m*) and crustal (*c*) components of Peteroa fumarolic gases can be computed according to the approach proposed by Sano and Wakita (1985), using the following values from Ozima and Podosek (2002): $(^3He/^4He)_a$ = 1 R/Ra, $(^4He/^{20}Ne)_a$ = 0.318, $(^3He/^4He)_m$ = 8 R/Ra, $(^4He/^{20}Ne)_m$ = 1,000, $(^3He/^4He)_c$ = 0.01 R/Ra, and $(^4He/^{20}Ne)_c$ = 1,000. Most fumarolic gases during the 2010–2021 period show a dominant He-magmatic component (70%–89%), whereas the crust component was 11%–29% and the atmospheric component accounts for <1% (Table 2). On the other hand, the 2012 fumarolic gases show a significantly lower fraction of the magmatic component (∼55%), slightly higher than the crustal component (∼44%). In general, the crustal contribution evidenced by the above calculations is consistent with the regional findings by Lages et al. (2021), who suggested a crustal control on light noble gas isotope variability along the Andean Volcanic Arc.

Similar to the Rc/Ra, the $\delta^{13}C$–CO_2 values are in the typical range of gases released from active volcanoes in subduction areas (Graham et al., 2014; Pineau & Javoy, 1983) except for the 2012 gases that are marked by a more negative isotopic signature (Figure 5).

Such a decrease in Rc/Ra and $\delta^{13}C$–CO_2 values occurring in 2012, already reported by Tassi et al. (2016), implies an increase in the crustal contribution in the source, which was interpreted as related to the degassing of a more evolved magmatic source of dacitic composition. The δD-H_2O and $\delta^{18}O$-H_2O values throughout the period are consistent with a dominant meteoric water source, including the 2011 data that were interpreted as related to fractionation due to vapor loss (Aguilera et al., 2016; Tassi et al., 2016).

7.2. Evolution of the Magmatic-Hydrothermal System in 2010–2021

The chemical composition of the Peteroa crater fumaroles is controlled by two factors: (a) degassing from an active magmatic system, which is evidenced by hyperacidic fumarolic fluids with high concentrations of HCl,
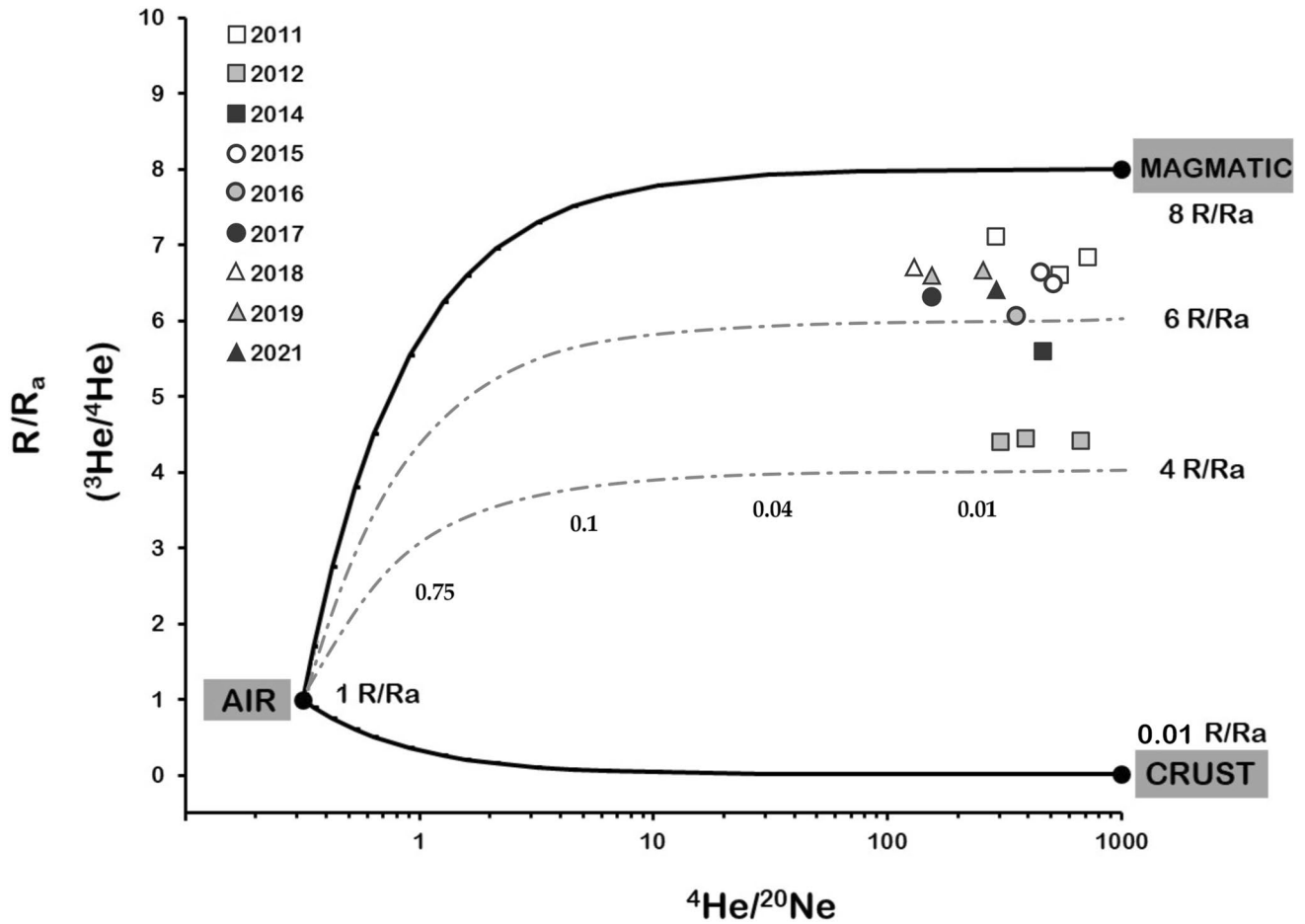
Figure 4. $^4He/^{20}Ne$ ratios and R/Ra ($^3He/^4He$) ratios observed in Peteroa summit fumarole samples. R/Ra values and $^4He/^{20}Ne$ ratios of Air, Crust, and Magmatic sources are from Ozima and Podosek (2002). Curves represent modeled theoretical mixing lines between air and the magmatic and crustal end-members.

HF, SO_2, and (b) fluid contribution from a relatively shallow aquifer, where gas–water–rock interactions generate the reduced gas species, such as H_2S, H_2, CO, and CH_4, which are typical of hydrothermal environment (Table 1). As ascending gases produced by the boiling of the hydrothermal reservoir pass through the fumarolic conduits, which are characterized by a relatively low permeability, they are affected by cooling and consequently water vapor condensation that controls the outlet fumarolic temperature near the boiling point.
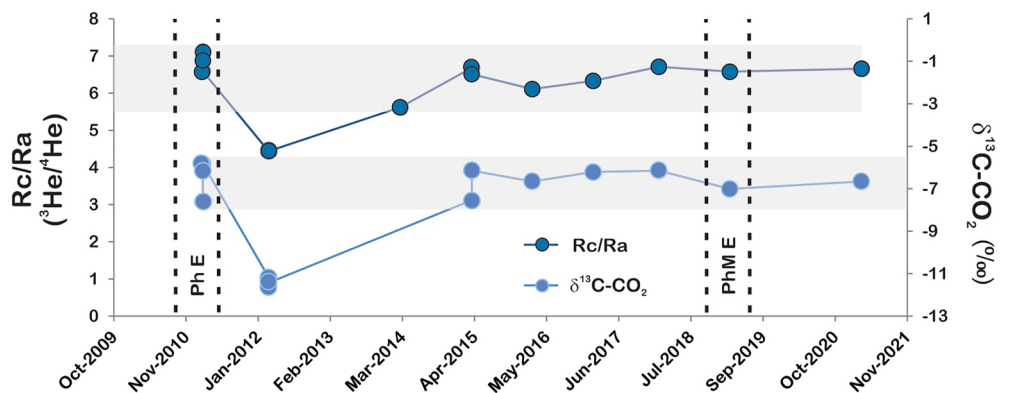
Figure 5. Time-series of Rc/Ra and $\delta^{13}C\text{-}CO_2$ (‰ vs. V-PDB) for all data from 2010 to 2021 of gases from the Peteroa crater fumaroles. Ph E and PhM E are phreatic and phreato-magmatic eruptions, respectively. Shaded areas indicate the narrow variation range of the deep magmatic signature, with one perturbation occurring in 2012.
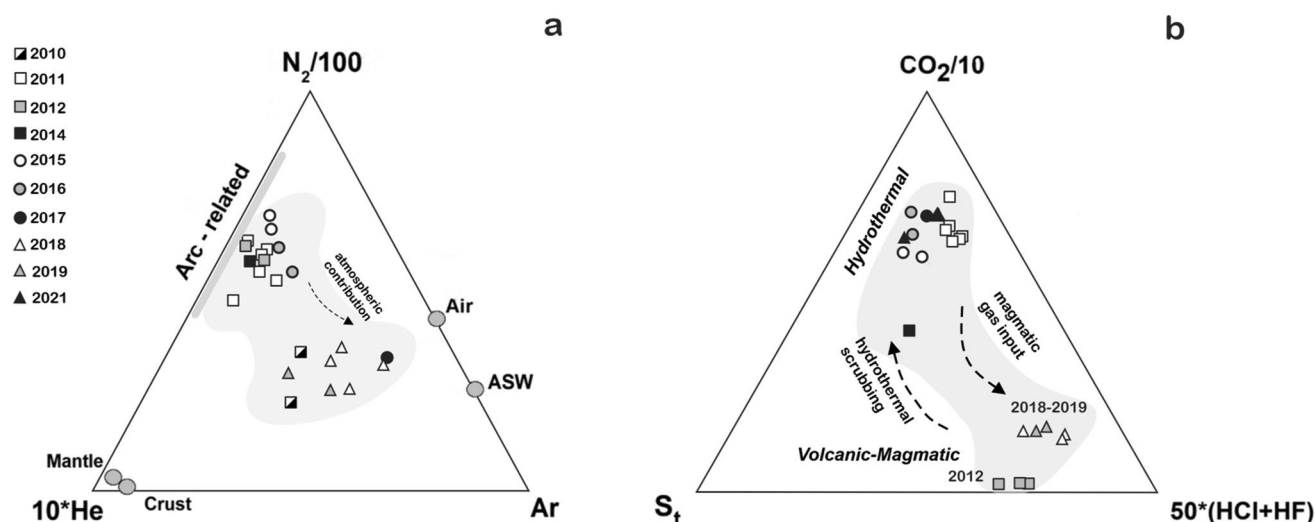
Figure 6. Ternary diagrams for fumarolic gas samples: (a) 10*He-N$_2$/100-Ar, the compositional fields for "Arc-related," "Mantle" and "Crust," and N$_2$/Ar ratios of "ASW" (air saturated water) and "Air" (Giggenbach, 1996) are reported, (b) CO$_2$/10–S$_t$–50*(HCl + HF), diagram of main acidic species showing the compositional field for "Hydrothermal" and "Volcanic-Magmatic" gases.

According to the N$_2$, He, and Ar relative contents (Figure 6a), the Peteroa fumarolic gases can be distinguished into two groups. The first group comprises gases from 2011 to 2016 and 2021, which exhibit relatively high N$_2$/Ar values (up to 1,400). These are typical of fluids from convergent plate boundaries (Giggenbach, 1996). As observed in gases from fumarolic discharges of other volcanoes of the SVZ (Barry et al., 2022, and references there in), such extremely high N$_2$-excess is likely related to thermal decomposition of organic material buried in the subducted sediments (Matsuo et al., 1978). The second group consists of gases from 2010 and 2017 to 2019, with N$_2$/Ar ratios ranging from those of Air Saturated Water (ASW) and air (Figure 6a). Noteworthy, the second group corresponds to pre-eruptive (2010, 2017, and 2018) and syn-eruptive (2019) periods. This suggests that during unrest periods, the Peteroa summit fumaroles are affected by increasing atmospheric contamination, likely favored by an increase in shallow permeability due to incipient fracturing. A similar process, likely due to the inflation of the volcano edifice caused by increasing pressure of the hydrothermal-magmatic fluids, has been observed in other volcanoes such as Turrialba (Costa Rica, de Moor et al., 2016) and Copahue (Argentina, Tassi et al., 2017).

Two groups of gases can be also distinguished on the basis of the relative concentrations of CO$_2$, S$_t$ (SO$_2$ + H$_2$S), HCl + HF, since gases collected in 2012, 2018 and 2019 are significantly enriched in magmatic-related species (HF, HCl, and SO$_2$) whit respect to the other gases (Figure 6b). Remarkably, during the phreatic eruption of 2010–2011, the gases exhibited relatively low contents of magmatic acid species (Figures 6b and 7). This phreatic eruption was likely triggered by the February 2010 Maule mega-earthquake of 8.8 Mw (Aguilera et al., 2016; Tassi et al., 2016). Possibly, due to the rapid succession of these events, there was not sufficient time for the gaseous emissions to develop a magmatic signature during this eruptive phase. Therefore, the 2012 post-eruptive magmatic signature would be generated by the arrival of magmatic-related gas species (SO$_2$, HCl, and HF) following a sudden release of the hydrothermal system after the phreatic eruptions. A comparable pattern of behavior related to the 2010 Maule mega-earthquake can be observed in the Copahue volcano (Caselli et al., 2016). This volcano is also located in the region and characterized by an important hydrothermal system and a hyperacid crater lake. After a period of over 10 years of quiescence, the Copahue volcano started displaying phreatic activity in 2011, followed by clear magmatic signs in 2012 (Agusto et al., 2017; Tassi et al., 2017). In a similar subduction-related tectonic setting in Central America, other comparable volcanoes experienced phreatic activity after the Mw 7.3 El Salvador and Mw 7.6 Nicoya earthquakes in 2012 (de Moor et al., 2017). Poás and Rincón de la Vieja have large hydrothermal systems, as evidenced by the presence of crater lakes, and they produced numerous phreatic eruptions following the earthquakes without a clear previous magmatic signal (Alvarado et al., 2016; Rizzo et al., 2016). However, attempts to establish a link between the 2010 Maule earthquake and the 2012 post-eruptive magmatic signature of Peteroa remain speculative with the limited seismic available data, as continuous seismic monitoring of the volcano only started in 2014 (Sections 3 and 4).
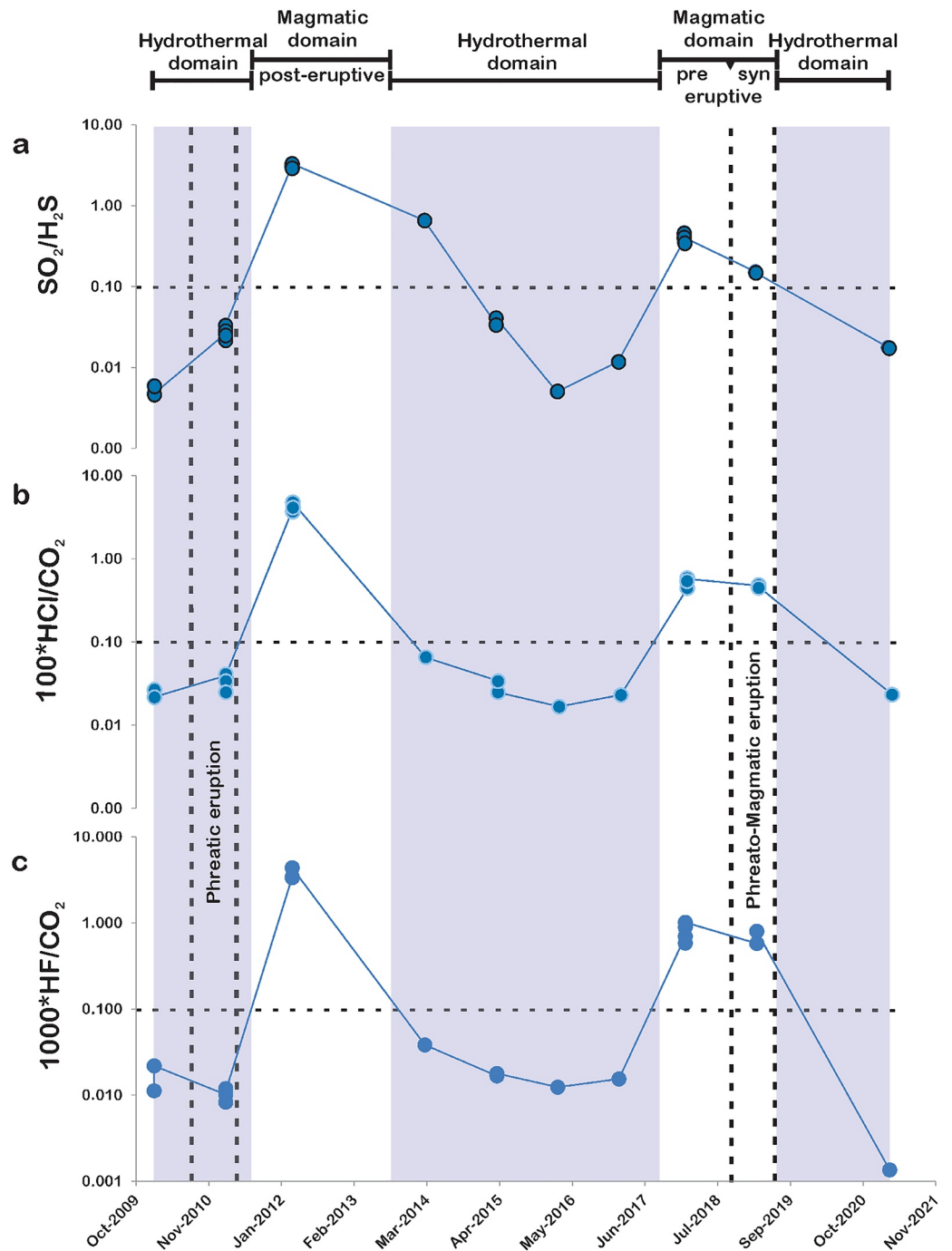
Figure 7. Time-series of (a) SO_2/H_2S, (b) $100*HCl/CO_2$, and (c) $1,000*HF/CO_2$ ratios from 2010 to 2021 fumarolic gases. The Phreatic and Phreato-magmatic eruptions (between thick dashed lines) are also reported. Thin dashed lines point out 0.1 ratio values. Magmatic domain (pre, syn, and post-eruptive) is defined when samples show the 3 ratios >0.1, simultaneously. Shaded areas indicate Hydrothermal domain.

On the other hand, the relatively high concentrations of SO_2, HCl, and HF in the 2018–2019 gases (Figure 7) are related to the phase of seismic unrest recorded prior to this period (Sections 3 and 4), causing a disturbance to the Peteroa magmatic-hydrothermal system.

Carbon dioxide is less soluble than SO_2, HCl, and HF in melts; therefore, a magmatic contribution from deeper mafic sources would drive the ratios of SO_2, HCl, and HF to CO_2 down by mixing with CO_2-rich gases. Thus, in

mafic magmatic systems, a rise in CO_2 contents during a pre-eruptive period is associated with the injection of new basaltic magma, which is usually followed by an increase in volcanic activity. However, no pulse of CO_2-rich magmatic gas was detected, as has been seen, for example, at Etna (Aiuppa et al., 2007), Redoubt (Werner et al., 2013), and Masaya (Aiuppa et al., 2017). This suggests that the intrusion of deeper basaltic magma is not the trigger for the eruption. Instead, CO_2 is the usually dominant species (Figure 6b), and the increase of SO_2, HCl, and HF during the pre and syn-eruptive 2018–2019 period (Figure 7) suggests a shallow magmatic source, similar to what was observed for Poás 2017 eruption (de Moor et al., 2019) and Taal 2020 eruption (Hernández et al., 2021). Enhanced magmatic degassing typically cause a partial vaporization and a decrease in the pH of hydrothermal aquifers, both of which can affect the capability of the hydrothermal reservoir to buffer the ascending magmatic gases (Capaccioni et al., 2016; Rouwet et al., 2017; Symonds et al., 2001; Tamburello et al., 2015). This explains the peaks of the HCl/CO_2 and HF/CO_2 ratios recorded in 2012, 2018, and 2019 (Figure 7).
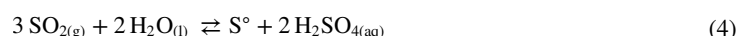
Under magmatic conditions, the S-bearing volatiles are controlled by the following reaction (Delmelle & Bernard, 2015; Giggenbach, 1987):

$$3 SO_2 + 7 H_2 \rightleftarrows H_2S + 2 S° + 6 H_2O \tag{2}$$

However, when magmatic fluids interact with a liquid dominated system, such as a hydrothermal reservoir, the relative contents of SO_2 and H_2S can be explained by the following reactions (e.g., Kusakabe et al., 2000):

$$4 SO_{2(g)} + 4 H_2O_{(l)} \rightleftarrows H_2S(g) + 3 H_2SO_{4(aq)} \tag{3}$$

and

$$3 SO_{2(g)} + 2 H_2O_{(l)} \rightleftarrows S° + 2 H_2SO_{4(aq)} \tag{4}$$

Therefore, considering that the chemistry of the Peteroa fumaroles is controlled by the interaction between magmatic and hydrothermal fluids, Reactions 3 and 4 superimpose on Reaction 2 and have the final control on the SO_2/H_2S ratios observed in the fumarolic discharges. In other words, periods of enhanced magmatic degassing, corresponding to a decrease in the hydrothermal contribution (Figure 6b), can be also traced by the evolution of the ratios between the two S-bearing gases (Figure 7a).

Hyperacid hydrothermal fluids can be almost transparent to volcanic gases, whereas less extreme hydrothermal conditions significantly scrub acidic volcanic gases (Capaccioni et al., 2016). For aquifers in extremely acidic conditions (pH 0 or <0) the reaction:

$$HCl_{(g)} \rightleftarrows Cl^-_{(aq)} + H^+_{(aq)} \tag{5}$$

moves to the left due to an H^+ excess with respect to Cl^-, favoring a HCl degassing. This implies that a low-temperature aquifer can release HCl as long as the aquifer is extremely acid. Reaction 5 also applies for HF. Furthermore, as a hot aquifer releases steam, the remnant liquid enriches in solutes and H^+ (i.e., salinity and acidity increase), leading to the fact that even SO_2 tends to degas from the hydrothermal aquifer, instead of remaining in the water phase as SO_4^{2-} or HSO_4^- (Rouwet et al., 2017). Thus, as a shallow hydrothermal reservoir experiences more acidic magmatic gas input, it may also release dissolved volatiles such as sulfur species, chlorine, and fluorine (Figure 6b).

According to their temporal evolution, $100*HCl/CO_2$, $1,000*HF/CO_2$ (hereafter HCl/CO_2 and HF/CO_2, respectively) and SO_2/H_2S ratios <0.1 (Figure 7) mark quiescent periods, when the hydrothermal system largely dominates over the magmatic fluid inputs ("Hydrothermal domain"), whereas ratios >0.1 corresponds to the crisis of the hydrothermal reservoir, showing a magmatic signature as a consequence of the increase in the magmatic gas species ("Magmatic domain").

During 2012, after the 2010–2011 eruptions, the SO_2/H_2S, HCl/CO_2, and HF/CO_2 ratios were about two orders of magnitude higher than quiescent periods. These peak ratios ranged between 2.9–3.3, 3.7–4.2, and 3.3–4.3, respectively (Table 1). During the 2018–2019 pre and syn-eruptive periods, these ratios developed a threshold with ranges of 0.15–0.46, 0.37–0.47, and 0.58–1.02, respectively.

On the whole, the compositional evolution recorded during the 11 years of observation has been dictated by the balance between fluid contributions from the magmatic system (HF, HCl, and SO_2) and the overhanging
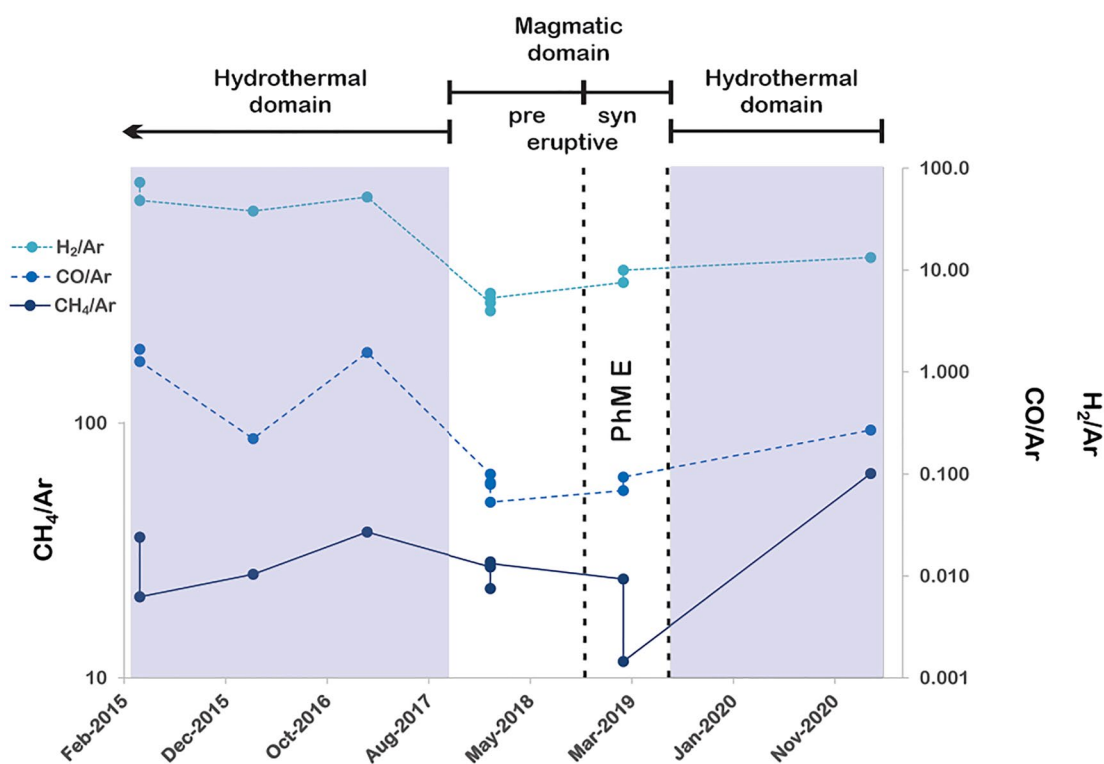
Figure 8. Time variations of CH_4/Ar, H_2/Ar, and CO/Ar ratios from 2015 to 2021 fumarolic gases. The Phreato-magmatic eruptions (PhM E, between thick dashed lines), the magmatic domain (pre and syn-eruptive), and the hydrothermal domain (shaded areas) are also reported.

hydrothermal reservoir (e.g., CO_2, H_2S). Therefore, the relative concentrations of these species can be considered as efficient geochemical precursors of possible eruptive events.

Similar to H_2S, CH_4 is favored by low temperature-reducing conditions, which is characteristic of hydrothermal environments (Giggenbach, 1991). For this reason, the variations of contents progress inversely to that of magmatic acidic gases. Figure 8 shows the reduced gases CH_4, H_2, and CO variations during the 2018–2019 eruption. Argon serves as a non-magmatic reference of atmospheric origin (Paonita et al., 2012) based on the measured $^{40}Ar/^{36}Ar$ ratios (Table 2) very close to the atmospheric ratio (i.e., 296, Sano et al., 2001) and much lower than the typical values of deep magmatic fluids ($^{40}Ar/^{36}Ar > 40,000$; Burnard et al., 1997; Fischer et al., 2005). Figure 8 depicts relatively higher ratio values during the "Hydrothermal Domain," likely favored by the reducing conditions. During the eruptive period, the CH_4/Ar ratios present a sharp decrease peak, possibly caused by increasing temperature and oxidizing redox conditions. After the eruption, the CH_4/Ar ratios increased again with the return of post-eruptive hydrothermal conditions. These syn- and post-eruptive period variations are not evident in the H_2/Ar and CO/Ar ratios. During the pre-eruptive period, these ratios decrease, but they remain constant until the "Hydrothermal Domain" in the post-eruptive period. The ambiguous behavior can be explained because the H_2 and CO contents are favored by both reducing redox conditions and increasing temperature (Giggenbach, 1996). However, a more comprehensive and focused investigation should be carried out to find a link between fluctuations in the composition of these species and the dynamics of the shallow hydrothermal system.

7.3. Conceptual Model for the 2018–2019 Eruption

During the seismic crisis lasting from January 2016 to February 2017, the observed peaks of VT events and the occurrence of LP and TR signals suggest that the Peteroa volcano underwent processes of rock fracturing and intense fluid circulation (Chouet & Matoza, 2013). Although the occurrence of a deep magmatic fluid input cannot be discarded, the concentrations of magmatic gases in fumarolic fluids were relatively low during this period (Figure 7), suggesting that the hydrothermal reservoir was able to scrub most of these highly soluble gas

species ("Hydrothermal Domain," Figure 9a). The hydrothermal conditions controlling the fumarolic emissions favored the relatively high contents of reduced gases (Figure 8).

The increase in LP and TR signals and the relatively low VT activity recorded in June–November 2017 may suggest that the Peteroa volcano was fed by a second pulse of hot deep fluids into the hydrothermal reservoir (Chouet & Matoza, 2013). According to this hypothesis, this pulse may have affected and depleted the hydrothermal reservoir favoring the uprising of magmatic gases up to the surface, as evidenced by their strong contents increase in February 2018 ("Magmatic domain," Figure 9b). This hypothesis is also supported by the observations carried out during the sampling campaign, reporting (a) a notable increase in the vapor and gas emission from Crater 3, and (b) the development of a new ephemeral fumarolic field between Craters 1 and 3 (Figure 1). The migration process of Peteroa's active vent from Crater 3 to Crater 1 in 2018 led to the development of a new fumarolic field. This change was also recognized by means of thermal anomalies in Craters 1 and 3 from satellite images (Aguilera et al., 2021; Romero et al., 2020).

From June 2018 to July 2019, the seismic activity was characterized by an increase in TR and LP signals at very shallow depths and in close proximity to Crater 1. These seismic signals would correspond to a third pulse of magmatic fluids, as also supported by the high proportions of juvenile material showing a trachyandesite composition (Romero et al., 2020). This disturbance likely triggered the phreatic explosions that occurred in June–November 2018 from Crater 1 and the phreato-magmatic eruption in December 2018. From December 2018 to February 2019, the column of gases and steam produced intense activity progressively enriched in ash, suggesting an effective consumption and retreating of the hydrothermal reservoir ("Magmatic domain," Figure 9c), in agreement with the dominant magmatic fluid contribution still characterizing the fumaroles in this period (Figure 7). After this eruptive phase up to 2021, the flow rate diminished significantly from both Crater 1 and the fumarolic fields. The nested Crater 1 vent was covered by detrital material from the crater walls where small fumaroles occurred (Figure 3) and the 2018 ephemeral fumarolic field between Crater1 and Crater 3 became an isolated small steaming ground emission. In agreement with these visual observations, the fumarolic gas composition showed an increase of the hydrothermal versus magmatic contribution (Figure 6b), suggesting a restoration of the conditions recorded in 2014–2017 with relatively higher contents of low temperature reduced gases ("Hydrothermal Domain," Figures 7 and 8).

8. Conclusions

This study investigates the evolution of fumarolic gases from Peteroa volcano during periods of quiescence, unrest, and eruptive activity. The observed changes in the chemical and isotopic composition of summit fumarole discharges from 2010 to 2021 were determined by the balance between magmatic and hydrothermal counterparts, which was repeatedly disturbed by new magmatic inputs from depth.

During quiescent periods, fumarolic activity showed relative low (<0.1) SO_2/H_2S, $100*/CO_2$, and $1,000*HF/CO_2$ ratios, which can be defined as "Hydrothermal domain." This is because the hydrothermal reservoir is able to scrub almost completely the hyper-acidic magmatic gas species. Low-temperature reduced gases, that is, H_2S and CH_4 are favored at these conditions, whereas the concentrations of CO and H_2, which are also favored by high temperature, are not consistent with increasing reducing conditions typical of a hydrothermal environment.

In contrast, during the pre- and syn-eruptive phases of 2018–2019 and the post-eruptive phase of 2012, magmatic gases significantly increased, defining "Magmatic domain" periods, as a consequence of the decrease and acidification of the hydrothermal system. The magmatic source temporarily changed in 2012, as suggested by the lowering of Rc/Ra and δ^{13}C-CO_2 values (Tassi et al., 2016), whereas it remained constant in the 2016–2021 period.

Combined geochemical and seismic data were used to reconstruct the evolution of the magmatic-hydrothermal system from 2016 to 2021, including the 2018–2019 eruptive phase. This conceptual model demonstrates the rapid response of the fumarolic emissions from the Peteroa summit to changes affecting the magmatic-hydrothermal plumbing system. Therefore, the geochemical monitoring, specifically focusing of the acidic gases as the most promising precursory parameters for eruptive (phreatic and phreatomagmatic) events, has proven to be an effective technique to track the evolution of volcanic activity at this volcano. However, considering the difficult access to the volcano summit, the application of remote sensing techniques in the future may represent a strong improvement of the surveillance program of this extremely active volcano.
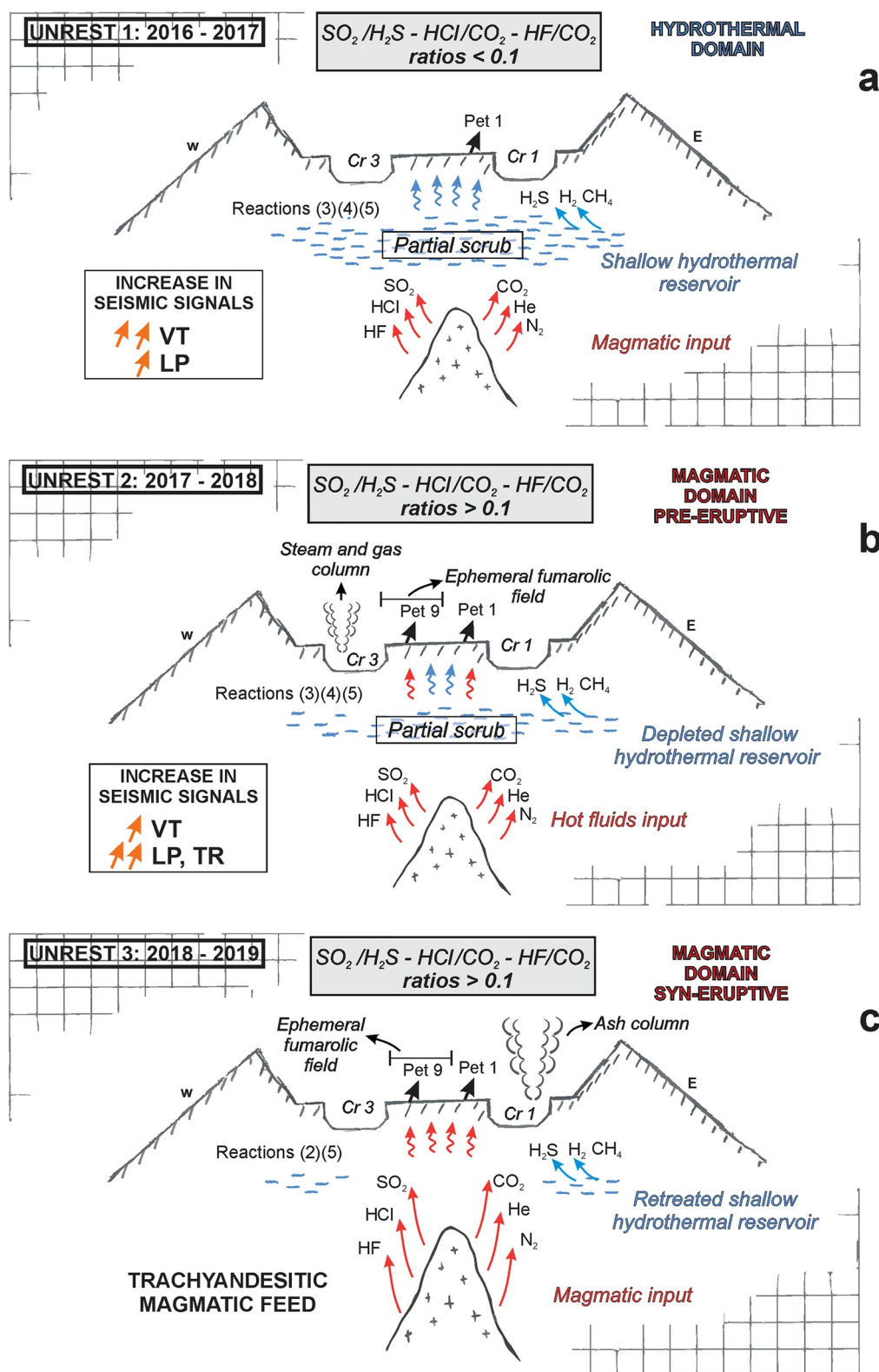
Figure 9. Schematic West to East cross section of Peteroa volcano. Geochemical conceptual model showing the evolution of the magmatic-hydrothermal system during the 3 unrest periods related to the 2018–2019 eruption. (a) Unrest 2016–2017, hydrothermal domain, (b) Unrest 2017–2018, pre-eruptive magmatic domain, (c) Unrest 2018–2019, syn-eruptive magmatic domain. Factor gas ratios as Figure 7.

Data Availability Statement

All data needed to evaluate the discussion and conclusions of this work are present in this paper and available from the institutional CONICET public repository (Agusto et al., 2023). Compiled data are from original papers, i.e., Tassi et al. (2016), Aguilera et al. (2016), and Romero et al. (2020).

References

Aguilera, F., Benavente, O., Gutiérrez, F., Romero, J., Saltori, O., González, R., et al. (2016). Eruptive activity of Planchón-Peteroa volcano for period 2010-2011, southern Andean volcanic zone, Chile. *Andean Geology*, *43*(1), 20–46. https://doi.org/10.5027/andgeov43n1-a02

Aguilera, F., Caro, J., & Layana, S. (2021). The evolution of Peteroa Volcano (Chile–Argentina) crater lakes between 1984 and 2020 based on Landsat and Planet Labs imagery analysis. *Frontiers in Earth Science*, *9*, 722056. https://doi.org/10.3389/feart.2021.722056

Agusto, M., Caselli, A., Daga, R., Varekamp, J., Trinelli, M. A., dos Santos Afonso, M., et al. (2017). The crater lake of Copahue volcano (Argentina): Geochemical and thermal changes over the last 2 decades. In T. En Obha, B. Capaccioni, & C. Cuadron (Eds.), *Geochemistry and geophysics of active volcanic lakes* (Vol. 437, pp. 107–130). Geological Society, London, Special Publications. https://doi.org/10.1144/SP437.16

Agusto, M., Nogués, V., Lamberti, M. C., Tassi, F., Llano, J., Carbajal, F., et al. (2021). Pre-eruptive geochemical changes of the Peteroa volcanic gases as precursor of the 2018-2019 eruption. In *IAVCEI, 1st CCVG virtual workshop 2021*. Retrieved from https://ccvg.iavceivolcano.org/event/1st-ccvg-virtual-workshop-2021/

Agusto, M., Tassi, F., Caselli, A., Vaselli, O., Rouwet, D., Capaccioni, B., et al. (2013). Gas geochemistry of the magmatic-hydrothermal fluid reservoir in the Copahue-Caviahue Volcanic Complex (Argentina). *Journal of Volcanology and Geothermal Research*, *257*, 44–56. https://doi.org/10.1016/j.jvolgeores.2013.03.003

Agusto, M. R., Lamberti, M. C. I., & Llano, J. (2023). Chemical and isotopic composition of fumarolic gases from the Peteroa volcano (Argentina-Chile) [Dataset]. Consejo Nacional de Investigaciones Científicas y Técnicas. http://hdl.handle.net/11336/208244

Aiuppa, A., Fischer, T., Plank, P., Robidoux, T. P., & Napoli, R. D. (2017). Along-arc, inter-arc and arc-to-arc variations in volcanic gas CO_2/S_T ratios reveal dual source of carbon in arc volcanism. *Earth-Science Reviews*, *168*, 24–47. https://doi.org/10.1016/j.earscirev.2017.03.005

Aiuppa, A., Moretti, R., Federico, C., Giudice, G., Gurrieri, S., Liuzzo, M., et al. (2007). Forecasting Etna eruptions by real-time observation of volcanic gas composition. *Geology*, *35*(12), 1115–1118. https://doi.org/10.1130/g24149a.1

Alvarado, G. E., Mele, D., Dellino, P., de Moor, J. M., & Avard, G. (2016). Are the ashes from the latest eruptions (2010–2016) at Turrialba volcano (Costa Rica) related to phreatic or phreatomagmatic events? *Journal of Volcanology and Geothermal Research*, *327*, 407–415. https://doi.org/10.1016/j.jvolgeores.2016.09.003

Barry, P. H., de Moor, J. M., Chiodi, A., Aguilera, F., Hudak, M. R., Bekaert, D. V., et al. (2022). The helium and carbon isotope characteristics of the Andean Convergent Margin. *Frontiers in Earth Science*, *10*. https://doi.org/10.3389/feart.2022.897267

Benavente, O. (2010). *Actividad hidrotermal asociada a los complejos volcánicos Planchón-Peteroa y Descabezado Grande-Quizapu- Cerro Azul, 36°S y 37°S, Zona volcánica sur, Chile* (p. 206). Memoria para optar al título de Geólogo, Universidad de Chile (inédita).

Benavente, O., Tassi, F., Reich, M., Aguilera, F., Capecchiacci, F., Gutiérrez, F., et al. (2015). Chemical and isotopic features of cold and thermal fluids discharged in the southern volcanic zone between 32.5°S and 36°S: Insights into the physical and chemical processes controlling fluid geochemistry in geothermal systems of Central Chile. *Chemical Geology*, *420*, 97–113. https://doi.org/10.1016/j.chemgeo.2015.11.010

Bobrowski, N., Kuhn, J., Lamberti, M. C., Agusto, M., García, S., Velazquez, G., et al. (2019). *Gas emission and composition measurements at two Andean volcanoes—Copahue and Peteroa*. EGU General Assembly 2019.

Bonali, F. L., Tibaldi, A., Corazzato, C., Tormey, D. R., & Lara, L. E. (2013). Quantifying the effect of large earthquakes in promoting eruptions due to stress changes on magma pathway: The Chile case. *Tectonophysics*, *583*, 54–67. https://doi.org/10.1016/j.tecto.2012.10.025

Burnard, P., Graham, D., & Turner, G. (1997). Vesicle-specific noble gas analyses of popping rock: Implications for primordial noble gases in the Earth. *Science*, *276*(5312), 568–571. https://doi.org/10.1126/science.276.5312.568

Capaccioni, B., Rouwet, D., & Tassi, F. (2016). HCl degassing from extremely acidic crater lakes: Empirical results from experimental determinations and implications for geochemical monitoring. In C. Caudron, B. Capaccioni, & T. Ohba (Eds.), *GSL special publications 437 geochemistry and geophysics of volcanic lakes*. https://doi.org/10.1144/SP437.12

Caselli, A., Agusto, M., Velez, M. L., Forte, P., Bengoa, C., Daga, R., et al. (2016). The 2012 eruption. In F. Tassi, O. Vaselli, & A. Caselli (Eds.), *Copahue Volcano* (pp. 61–77). Springer International Publishing AG. https://doi.org/10.1007/978-3-662-48005-2_4

Chiodini, G., Giudicepietro, F., Vandemeulebrouck, J., Aiuppa, A., Caliro, S., De Cesare, W., et al. (2017). Fumarolic tremor and geochemical signals during a volcanic unrest. *Geology*, *45*(12), 1131–1134. https://doi.org/10.1130/G39447.1

Chouet, B. A., & Matoza, R. S. (2013). A multi-decadal view of seismic methods for detecting precursors of magma movement and eruption. *Journal of Volcanology and Geothermal Research*, *252*, 108–175. https://doi.org/10.1016/j.jvolgeores.2012.11

Christenson, B. W., White, S., Britten, K., & Scott, B. J. (2017). Hydrological evolution and chemical structure of a hyper-acidic spring-lake system on Whakaari/White Island, NZ. *Journal of Volcanology and Geothermal Research*, *346*, 180–211. https://doi.org/10.1016/j.jvolgeores.2017.1006.1017

Coleman, M., Shepherd, T., Rouse, J., & Moore, G. (1982). Reduction of water with zinc for hydrogen isotope analysis. *Analytical Chemistry*, *54*(6), 993–995. https://doi.org/10.1021/ac00243a035

Delmelle, P., & Bernard, A. (2015). The remarkable chemistry of sulfur in hyper-acid crater lakes: A scientific tribute to Bokuichiro Takano and Minoru Kusakabe. In D. Rouwet, B. Christenson, F. Tassi, & J. Vandemeulebrouck (Eds.), *Volcanic lakes* (pp. 239–260). Springer. https://doi.org/10.1007/978-3-642-36833-2_10

de Moor, J. M., Aiuppa, A., Avard, G., Wehrmann, H., Dunbar, N., Muller, C., et al. (2016). Turmoil at Turrialba Volcano (Costa Rica): Degassing and eruptive processes inferred from high-frequency gas monitoring. *Journal of Geophysical Research: Solid Earth*, *121*(8), 5761–5775. https://doi.org/10.1002/2016JB013150

de Moor, J. M., Kern, C., Avard, G., Muller, C., Aiuppa, A., Saballos, A., et al. (2017). A new sulfur and carbon degassing inventory for the Southern Central American Volcanic Arc: The importance of accurate time-series data sets and possible tectonic processes responsible for temporal variations in arc-scale volatile emissions. *Geochemistry, Geophysics, Geosystems*, *18*(12), 4437–4468. https://doi.org/10.1002/2017GC007141

de Moor, J. M., Stix, J., Avard, G., Muller, C., Corrales, E., Diaz, J. A., et al. (2019). Insights on hydrothermal_magmatic interactions and eruptive processes at Poás volcano (Costa Rica) from high_frequency gas monitoring and drone measurements. *Geophysical Research Letters*, *46*(3), 1293–1302. https://doi.org/10.1029/2018GL080301

Epstein, S., & Mayeda, T. (1953). Variation of the $^{18}O/^{16}O$ ratio in natural waters. *Geochimica et Cosmochimica Acta*, *4*(5), 213–224. https://doi.org/10.1016/0016-7037(53)90051-9

Evans, W., White, L., & Rapp, J. (1998). Geochemistry of some gases in hydrothermal fluids from the southern Juan de Fuca Ridge. *Journal of Geophysical Research*, *15*, 305–313.

Fischer, T. P., Ramírez, C. J., Mora, A. R., Hilton, D. R., Barnes, J. D., Sharp, Z. D., et al. (2015). Temporal variations in fumarole gas chemistry at Poás volcano, Costa Rica. *Journal of Volcanology and Geothermal Research*, *294*, 56–70. https://doi.org/10.1016/j.jvolgeores.2015.02.002

Fischer, T. P., Takahata, N., Sano, Y., Sumino, H., & Hilton, D. R. (2005). Nitrogen isotopes of the mantle: Insights from mineral separates. *Geophysical Research Letters*, *32*(11), L11305. https://doi.org/10.1029/2005GL022792

Forte, P., Ramires, A., De Abrantes, L., Llano, J., Dominguez, L., Carbajal, F., et al. (2022). La erupción no será transmitida: características, impactos y asistencia durante el ciclo eruptivo 2018-2019 del volcán Peteroa, Argentina. *Revista de la Asociación Geológica Argentina*, *79*(1), 47–71.

Giggenbach, W. F. (1987). Redox processes governing the chemistry of fumarolic gas discharges from White Island, New Zealand. *Applied Geochemistry*, *2*, 143–161. https://doi.org/10.1016/0883-2927(87)90030-8

Giggenbach, W. F. (1991). Chemical techniques in geothermal exploration. In F. D'Amore (Ed.), *Application of geochemistry in geothermal reservoir development* (pp. 119–144). UNITAR.

Giggenbach, W. F. (1996). Chemical composition of volcanic gases. In R. Scarpa, & R. Tilling (Eds.), *Monitoring and mitigation of volcano hazard* (pp. 222–256). Springer-Verlag.

González-Ferrán, O. (1995). *Volcanes de Chile* (p. 639). Instituto Geográfico Militar.

Graham, D. W., Hanan, B. B., H´emond, C., Blichert-Toft, J., & Albar`ede, F. (2014). Helium isotopic textures in Earth's upper mantle. *Geochemistry, Geophysics, Geosystems*, *15*(5), 2048–2074. https://doi.org/10.1002/2014GC005264

Haller, M., & Risso, C. (2011). La erupción del volcán Peteroa (35°15′S, 70°1′O) del 4 de septiembre de 2010. *Revista de la Asociación Geológica Argentina*, *68*, 295–305.

Hernández, P. A., Melián, G. V., Asensio-Ramos, M., Padrón, E., Sumino, H., Pérez, N. M., et al. (2021). Geochemical and isotopic evidence of volcanic plumbing system processes from fumarolic gases of Taal volcano, Philippines, prior to the January 2020 eruption. *Chemical Geology*, *574*, 120216. https://doi.org/10.1016/j.chemgeo.2021.120216

Hildreth, W., Grunder, A., & Drake, R. (1984). The Loma Seca Tuff and the Calabozos caldera: A major ash-flow and caldera complex in the southern Andes of central Chile. *Geological Society of America Bulletin*, *95*(1), 45–54. https://doi.org/10.1130/0016-7606(1984)95<45:tlstat>2.0.co;2

Klug, J. D., Singer, B. S., Jicha, B. R., Ramirez, A., & Sruoga, P. (2018). $^{40}Ar/^{39}Ar$ geochronology and geochemical evolution of Planchon-Peteroa volcanic complex. In *Paper presented at GSA annual meeting*.

Kusakabe, M., Komoda, Y., Takano, B., & Abiko, T. (2000). Sulfur isotopic effects in the disproportionation reaction of sulfur dioxide in hydrothermal fluids: Implications for the $\delta^{34}S$ variations of dissolved bisulphate and elemental sulfur from active crater lakes. *Journal of Volcanology and Geothermal Research*, *97*(1–4), 287–307. https://doi.org/10.1016/s0377-0273(99)00161-4

Lages, J., Rizzo, A. L., Aiuppa, A., Robidoux, P., Aguilar, R., Apaza, F., & Masias, P. (2021). Crustal controls on light noble gas isotope variability along the Andean Volcanic Arc. *Geochemical Perspectives Letters*, *19*, 45–49. https://doi.org/10.7185/geochemlet.2134

Lamberti, M. C., Agusto, M., Llano, J., Nogués, V., Vélez, M. L., Albite, J. M., et al. (2021). Soil CO_2 flux baseline in Planchón—Peteroa volcanic complex, southern Andes, Argentina. *Journal of South American Earth Sciences*, *105*, 102930. ALVO Conference Special Issue. https://doi.org/10.1016/j.jsames.2020.102930

Llano, J., Nogués, V., Agusto, M., Lamberti, M. C., Sierra, D., García, S., et al. (2021). Geoquímica de las aguas vinculadas al Complejo Volcánico Planchón-Peteroa, Mendoza-Argentina. *Revista de la Asociación Geológica Argentina*, *79*(3). https://revista.geologica.org.ar/raga/article/view/1471

Mamyrin, B. A., & Tolstikhin, I. N. (1984). *Helium isotopes in nature*. Elsevier.

Matsuo, S., Suzuki, M., & Mizutani, Y. (1978). Nitrogen to argon ratio in volcanic gases. *Advances in Earth and Planetary Sciences Letters*, *3*, 17–25.

McNutt, S. R. (2000). Synthesis of volcano monitoring. In H. En Sigurdsson, B. Houghton, S. R. McNutt, H. Rymer, & J. Stix (Eds.), *Encyclopedia of volcanoes* (pp. 1167–1185). Academic Press.

Melián, G. V., Hernández, P. A., Pérez, N. M., Asensio-Ramos, M., Padrón, E., Alonso, M., et al. (2021). Insights from fumarole gas geochemistry on the recent volcanic unrest of Pico do Fogo, Cape Verde. *Frontiers in Earth Science*, *9*, 631190. https://doi.org/10.3389/feart.2021.631190

Menyailov, I. A., Nikitina, L. P., Shapar, V. N., & Pilipenko, V. P. (1986). Temperature increase and chemical change of fumarolic gases at Momotombo Volcano, Nicaragua, in 1982–1985; are these indicators of a possible eruption? *Journal of Geophysical Research B*, *91*(12), 12199–12214. https://doi.org/10.1029/jb091ib12p12199

Mick, E., Stix, J., de Moor, J. M., & Geoffroy Avard, G. (2021). Hydrothermal alteration and sealing at Turrialba volcano, Costa Rica, as a mechanism for phreatic eruption triggering. *Journal of Volcanology and Geothermal Research*, *416*, 107297. https://doi.org/10.1016/j.jvolgeores.2021.107297

Montegrossi, G., Tassi, F., Vaselli, O., Buccianti, A., & Garofalo, K. (2001). Sulfur species in volcanic gases. *Analytical Chemistry*, *73*(15), 3709–3715. https://doi.org/10.1021/ac001429b

Moreira, M., Kunz, J., & Allègre, C. (1998). Rare gas systematics in popping rock: Isotopic and elemental compositions in the upper mantle. *Science*, *279*(5354), 1178–1181. https://doi.org/10.1126/science.279.5354.1178

Moretti, R., Arienzo, I., Civetta, L., Orsi, G., & Papale, P. (2013). Multiple magma degassing sources at an explosive volcano. *Earth and Planetary Science Letters*, *367*, 95–104. https://doi.org/10.1016/j.epsl.2013.02.013

Nakamichi, H., Kumagai, H., Nakano, M., Okubo, M., Kimata, F., Ito, Y., & Obara, K. (2009). Source mechanism of a very-long-period event at Mt Ontake, central Japan: Response of a hydrothermal system to magma intrusion beneath the summit. *Journal of Volcanology and Geothermal Research*, *187*(3-4), 167–177. https://doi.org/10.1016/j.jvolgeores.2009.09.006

Naranjo, J., & Haller, M. (2002). Erupciones principalmente explosivas del volcán Planchón, Andes del sur (35°15′S). *Revista Geológica de Chile*, *29*(1), 93–113. https://doi.org/10.4067/s0716-02082002000100006

Naranjo, J., Haller, M., Ostera, H., Pesce, A., & Sruoga, P. (1999). *Geología y Peligros del Complejo Volcánico Planchon–Peteroa, Andes del Sur (35°15′S), Región del Maule, Chile, Provincia de Mendoza, Argentina* (Vol. 52). Servicio Nacional de Geología y Minería.

Nogués, V. (2019). *Geología del flanco oriental del volcán Peteroa, provincia de Mendoza, y geoquímica de las emisiones fluidas del sistema volcánico-hidrotermal* (p. 156). Tesis Final de Licenciatura. Universidad de Buenos Aires.

Ohba, T., Yaguchi, M., Nishino, K., Numanami, N., Daita, Y., Sukigara, C., et al. (2019). Time variations in the chemical and isotopic composition of fumarolic gases at Hakone volcano, Honshu Island, Japan, over the earthquake swarm and eruption in 2015, interpreted by magma sealing model. *Earth Planets and Space*, *71*(1), 48. https://doi.org/10.1186/s40623-019-1027-5

Ozima, M., & Podosek, F. A. (1983). *Noble gas Geochemistry*. Cambridge University Press.

Ozima, M., & Podosek, F. A. (2002). *Noble gas Geochemistry*. Cambridge University Press.

Paonita, A., Caracausi, A., Iacono-Marziano, G., Martelli, M., & Rizzo, A. (2012). Geochemical evidence for mixing between fluids exsolved at different depths in the magmatic system of Mt Etna (Italy). *Geochimica et Cosmochimica Acta*, *84*, 380–394. https://doi.org/10.1016/j.gca.2012.01.028

Pineau, F., & Javoy, M. (1983). Carbon isotopes and concentration in mid-oceanic ridge basalts. *Earth and Planetary Science Letters*, *62*(2), 239–257. https://doi.org/10.1016/0012-821x(83)90087-0

Poreda, R. J., & Craig, H. (1989). Helium isotope ratios in circum-Pacific volcanic arcs. *Nature*, *338*(6215), 473–478. https://doi.org/10.1038/338473a0

Rizzo, A., Barberi, F., Carapezza, M. L., Di Piazza, A., Francalanci, L., Sortino, F., & D'Alessandro, W. (2015). New mafic magma refilling a quiescent volcano: Evidence from He-Ne-Ar isotopes during the 2011–2012 unrest at Santorini, Greece. *Geochemistry, Geophysics, Geosystems*, *16*(3), 798–814. https://doi.org/10.1002/2014gc005653

Rizzo, A. L., Caracausi, A., Chavagnac, V., Nomikou, P., Polymenakou, P. N., Mandalakis, M., et al. (2019). Geochemistry of CO_2-rich gases venting from submarine volcanism: The case of Kolumbo (Hellenic Volcanic Arc, Greece). *Frontiers in Earth Science*, *7*, 60. https://doi.org/10.3389/feart.2019.00060

Rizzo, A. L., Di Piazza, A., de Moor, J. M., Alvarado, G., Avard, E. G., Carapezza, M. L., & Mora, M. (2016). Eruptive activity at Turrialba volcano (Costa Rica): Inferences from $^3He/^4He$ in fumaroles gases and chemistry of ejected products. *Geochemistry, Geophysics, Geosystems*, *17*(11), 4478–4494. https://doi.org/10.1002/2016GC006525

Rizzo, A. L., Robidoux, P., Aiuppa, A., & Di Piazza, A. (2022). $^3He/^4He$ signature of magmatic fluids from Telica (Nicaragua) and Baru (Panama) volcanoes, Central American Volcanic Arc. *Applied Sciences*, *12*(9), 4241. https://doi.org/10.3390/app12094241

Romero, J. E., Aguilera, F., Delgado, F., Guzmán, D., Van Eaton, A. R., Luengo, N., et al. (2020). Combining ash analyses with remote sensing to identify juvenile magma involvement and fragmentation mechanisms during the 2018/19 small eruption of Peteroa volcano (Southern Andes). *Journal of Volcanology and Geothermal Research*, *402*, 106984. https://doi.org/10.1016/j.jvolgeores.2020.106984

Roulleau, E., Tardani, D., Sano, Y., Takahata, N., Vinet, N., Bravo, F., et al. (2016). New insight from noble gas and stable isotopes of geothermal/hydrothermal fluids at Caviahue-Copahue Volcanic Complex: Boiling steam separation and water-rock interaction at shallow depth. *Journal of Volcanology and Geothermal Research*, *328*, 70–83. https://doi.org/10.1016/j.jvolgeores.2016.10.007

Rouwet, D., Hidalgo, S., Joseph, E., & Gonzalez-Ilana, G. (2017). Fluid geochemistry and volcanic unrest: Dissolving the haze in time and space. In J. Gottsmann, J. Neuberg, & B. Scheu (Eds.), *Volcanic unrest* (pp. 221–239). Springer International Publishing AG. https://doi.org/10.1007/11157_2017_12

Sano, Y., Takahata, N., Nishio, Y., Fischer, T. P., & Williams, S. N. (2001). Volcanic flux of nitrogen from the Earth. *Chemical Geology*, *171*(3–4), 263–271. https://doi.org/10.1016/s0009-2541(00)00252-7

Sano, Y., & Wakita, H. (1985). Geographical distribution of $^3He/^4He$ ratios in Japan: Implications for arc tectonics and incipient magmatism. *Journal of Geophysical Research*, *90*(B10), 8729–8741. https://doi.org/10.1029/jb090ib10p08729

Scarpa, R., & Tilling, R. I. (1996). *Monitoring and mitigation of volcano hazards*. Springer-Verlag.

SEGEMAR-OAVV. (2019-2021). Monitoreo Volcánico Planchón-Peteroa. Retrieved from https://oavv.segemar.gob.ar/monitoreo-volcanico/planchon-peteroa/

SERNAGEOMIN-OVDAS. (2010-2021). Complejo Volcánico Planchón-Peteroa. Retrieved from https://rnvv.sernageomin.cl/complejo-volcanico-planchon-peteroa/

Symonds, R. B., Gerlach, T. M., & Reed, M. H. (2001). Magmatic gas scrubbing: Implications for volcano monitoring. *Journal of Volcanology and Geothermal Research*, *108*(1–4), 303–341. https://doi.org/10.1016/s0377-0273(00)00292-4

Tamburello, G., Agusto, M., Caselli, A., Tassi, F., Vaselli, O., Calabrese, S., et al. (2015). Intense magmatic gas leakage through the Copahue crater lake. *Journal of Geophysical Research: Solid Earth*, *120*(9), 6071–6084. https://doi.org/10.1002/2015JB012160

Tardani, D., Reich, M., Roulleau, E., Takahata, N., Sano, Y., Pérez-Flores, P., et al. (2017). Exploring the structural controls on Helium, Nitrogen and Carbon isotope signatures in hydrothermal fluids along an intra-arc fault system. *Geochimica et Cosmochimica Acta*, *184*, 193–211. https://doi.org/10.1016/j.gca.2016.04.031

Tassi, F., Aguilera, F., Benavente, O., Paonita, A., Chiodini, G., Caliro, S., et al. (2016). Geochemistry of fumarolic fluids from Peteroa volcano (Argentina-Chile) in 2010-2015: Insights into compositional changes related to the fluid source region. *Chemical Geology*, *432*, 41–53. https://doi.org/10.1016/j.chemgeo.2016.04.007

Tassi, F., Agusto, M., Lamberti, C., Caselli, A., Pecoraino, G., Caponi, C., et al. (2017). The 2012-2016 eruptive cycle at Copahue volcano (Argentina) versus the peripheral gas manifestations: Hints from the chemical and isotopic features of fumarolic fluids. *Bulletin of Volcanology*, *79*(10), 1–14. https://doi.org/10.1007/s00445-017-1151-7

Tilling, R. I. (2003). Volcano monitoring and eruption warnings. In J. Zschau, & A. N. Küppers (Eds.), *Early warning systems for natural disaster reduction* (pp. 505–510). Springer-Verlag.

Todesco, M. (2009). Signals from the Campi Flegrei hydrothermal system: Role of a "magmatic" source of fluids. *Journal of Geophysical Research*, *114*(B5), B05201. https://doi.org/10.1029/2008JB006134

Tormey, D. R., Frey, F. A., & López, L. (1995). Geochemistry of the active Azufre-Planch´on-Peteroa volcanic complex, Chile (35°15′S): Evidence for multiple sources and processes in a Cordilleran arc magmatic system. *Journal of Petrology*, *36*(2), 265–298. https://doi.org/10.1093/petrology/36.2.265

Vaselli, O., Tassi, F., Duarte, E., Fernandez, E., Poreda, R., & Delgado Huertas, A. (2010). Evolution of fluid geochemistry at the Turrialba volcano (Costa Rica) from 1998 to 2008. *Bulletin of Volcanology*, *72*(4), 397–410. https://doi.org/10.1007/s00445-009-0332-4

Vaselli, O., Tassi, F., Montegrossi, G., & Capaccioni, B. (2006). Sampling and analysis of fumarolic gases. *Acta Vulcanologica*, *18*, 65–76.

Vigide, N., Yagupsky, D., Barcelona, H., Agusto, M., & Caselli, A. (2020). Structural analysis of the Planchón-Peteroa Volcanic Complex: Insights for the geothermal system. *Journal of South American Earth Sciences*, *104*, 102856. https://doi.org/10.1016/j.jsames.2020.102856

Villemant, B., Komorowski, J. C., Dessert, C., Michel, A., Crispi, O., Hammouya, G., et al. (2014). Evidence for a new shallow magma intrusion at La Soufrière of Guadeloupe (Lesser Antilles). *Journal of Volcanology and Geothermal Research*, *285*, 247–277. https://doi.org/10.1016/j.jvolgeores.2014.08.002

Werner, C., Kelly, P. J., Doukas, M., Lopez, T., Pfeffer, M., McGimsey, R., & Neal, C. (2013). Degassing of CO_2, SO_2, and H_2S associated with the 2009 eruption of Redoubt Volcano, Alaska. *Journal of Volcanology and Geothermal Research*, *259*, 270–284. https://doi.org/10.1016/j.jvolgeores.2012.04.012

Zelenski, M., & Taran, Y. (2011). Geochemistry of volcanic and hydrothermal gases of Mutnovsky volcano, Kamchatka: Evidence for mantle, slab and atmosphere contributions to fluids of a typical arc volcano. *Bulletin of Volcanology*, *73*(4), 373–394. https://doi.org/10.1007/s00445-011-0449-0